

Efficient Subgroup Analysis via Optimal Trees with Global Parameter Fusion

Zhongming Xie¹, Joseph Giorgio², and Jingshen Wang¹

Division of Biostatistics, University of California, Berkeley¹

Helen Wills Neuroscience Institute, University of California, Berkeley²

February 5, 2026

Abstract

Identifying and making statistical inferences on differential treatment effects—commonly known as subgroup analysis in clinical research—is central to precision health. Subgroup analysis allows practitioners to pinpoint populations for whom a treatment is especially beneficial or protective, thereby advancing targeted interventions. Tree-based recursive partitioning methods are widely used for subgroup analysis due to their interpretability. Nevertheless, these approaches encounter significant limitations, including suboptimal partitions induced by greedy heuristics and overfitting from locally estimated splits, especially under limited sample sizes. To address these limitations, we propose a fused optimal causal tree method that leverages mixed-integer optimization (MIO) to facilitate precise subgroup identification. Our approach ensures globally optimal partitions and introduces a parameter-fusion constraint to facilitate information sharing across related subgroups. This design substantially improves subgroup discovery accuracy and enhances statistical efficiency. We provide theoretical guarantees by rigorously establishing out-of-sample risk bounds and comparing them with those of classical tree-based methods. Empirically, our method consistently outperforms popular baselines in simulations. Finally, we demonstrate its practical utility through a case study on the Health and Aging Brain Study–Health Disparities (HABS-HD) dataset, where our approach yields clinically meaningful insights.

1 Introductions

1.1 Motivation and Challenges

Alzheimer’s disease (AD) represents a critical public health burden. Fortunately, recent successful trials of Lecanemab and Donanemab (Van Dyck et al., 2023; Sims et al., 2023) have shown that reducing cortical Amyloid-beta plaques ($A\beta$), a primary pathology of AD, can produce measurable improvements in cognitive decline. However, the progression of AD pathology and its impact on cognition can vary substantially across populations with distinct genetic profiles and tau levels. For example, studies on Lecanemab reported limited cognitive benefits among subgroups such as females, non-white participants, and APOE4 carriers (Van Dyck et al., 2023), while the Donanemab trial showed no significant effects in a prespecified cohort with high tau pathology (Sims et al., 2023). These findings underscore the need for statistical methodologies capable of uncovering heterogeneity in AD pathologies, offering insights for personalized $A\beta$ -lowering treatment strategies.

Identifying such heterogeneity remains a central challenge in AD research. Recursive partitioning tree-based methods (Su et al., 2009; Loh et al., 2015) are widely used to partition the covariate space into interpretable subgroups, facilitating the discovery of heterogeneous pathologies. Despite their popularity, applying these methods to AD studies poses several challenges:

(1) *Suboptimal and unstable subgroup partitions that fail to capture true heterogeneity, especially in underrepresented populations with limited sample sizes.* Most biomedical studies are run in urban centers, and the high transportation costs of traveling to these sites discourage participation from rural communities. As a result, Alzheimer’s disease cohort studies often under-represent these populations and include only small sample sizes for them. With such limited data, tree-based methods for subgroup identification become especially unstable and prone to spurious splits, making it difficult to detect true heterogeneity. This is because these methods rely on greedy heuristics, generating splits in isolation without considering

the possible impact of future splits in the tree (Bertsimas and Dunn, 2017). Such instability could misrepresent the underlying heterogeneity of AD subpopulations, leading to incorrect conclusions about the heterogeneous AD pathologies.

(2) *Rare risk alleles such as APOE- ϵ 4 introduce critical heterogeneity in AD, yet their scarcity demands that analyses borrow information across subgroups to attain reliable insights.* AD is tightly linked to genetic risk factors: rare alleles such as APOE- ϵ 4—carried by only about 5% of the population—likely introduce substantial heterogeneity. When the entire study sample size is already small, analyzing AD pathology solely within allele carriers becomes impractical unless we let subgroups with different pathologies share information (“borrow strength”) across one another. However, standard recursive-partitioning trees cannot borrow strength: each split is chosen solely from the data in its local node, disregarding information elsewhere in the tree and missing the dataset’s global structure (Tan et al., 2022).

1.2 Our Solution and Contributions

To address these challenges and enhance the discovery of more accurate and informative AD subpopulations, we propose a *fused optimal causal tree*, which offers two primary contributions over existing tree-based subgroup analysis methods:

Data efficient and globally optimal subgroup partitions achieved by mixed integer optimization: Rather than employing greedy tree-based methods, we frame the subgroup discovery problem as a comprehensive mixed integer optimization (MIO) problem, with an objective function tailored to promote heterogeneous causal discovery of AD subpopulations. This formulation allows us to construct the optimal causal tree by addressing a single comprehensive optimization problem, rather than decomposing it into isolated sub-problems solved greedily and resulting in sub-optimal solutions (Algorithm 1). We also provide a theoretical analysis to demonstrate that the proposed method consistently uncovers true subgroup partitions without requiring an excessive tree depth (Theorem 4.2). In contrast, conventional greedy-based trees, like CART, often require infinite depth to achieve

similar consistency.

Allow information sharing between subgroups to encourage more informative subgroup discovery and enhance statistical estimation efficiency: To facilitate between-subgroup information sharing, we impose a parameter-fusion constraint on the leaf nodes, so covariate effects can align across branches. Greedy tree algorithms cannot handle such global constraints because they optimize splits one node at a time, but our mixed-integer programming formulation embeds fusion directly into the full optimization, letting the entire dataset inform subgroup boundaries and treatment-effect estimates. As indicated by our simulations in Section 5, this fusion constraint not only improves the accuracy of subgroup identification but also produces more efficient causal estimates. With this method, we can provide more reliable insights into which AD subpopulations are most likely to benefit from specific treatments.

1.3 Related Literature

Regression-based subgroup identification methods have gained popularity in subgroup analysis due to their ability to model heterogeneity through interaction terms. Notably, Tian et al. (2014) and Shen and He (2015) incorporate interactions between the treatment and pre-specified subgroup indicators within regression models. By adopting a variable selection perspective, these methods aim to identify significant interactions that indicate differential treatment effects across subgroups. However, a potential limitation is that subgroup indicators often cannot be pre-specified in practice. This constraint renders regression-based methods more restrictive compared to tree-based approaches, which can automatically discover relevant subgroups from the data without prior specification.

Alternatively, as discussed earlier in the manuscript, researchers have proposed recursive partitioning tree-based approaches to overcome these limitations. Su et al. (2009), Athey and Imbens (2016), Wager and Athey (2018), Hill (2011), Zeldow et al. (2019), and Hahn et al. (2020) develop methods that identify subgroups by recursively partitioning the data

based on baseline confounders. These tree-based models are adept at capturing complex interactions and nonlinear relationships inherent in heterogeneous treatment effects. Ting and Linero (2023) further extends the Bayesian Additive Regression Trees (BART) method to identify heterogeneous causal mediation effects involving a single mediator, showcasing the versatility of tree-based methods in causal inference. Despite their strengths, classical tree-based approaches often rely on heuristics for making split decisions in isolation, which may not yield globally optimal solutions. Similarly, clustering algorithms like k -means and Gaussian mixture models have been used to first identify subgroups and then estimate causal parameters Xue et al. (2022), but these methods also face challenges in achieving global optimality.

Recent literature has focused on enhancing the efficiency and optimality of classification and regression trees by employing advanced optimization techniques. Dynamic programming methods have been utilized by Demirović et al. (2022), Lin et al. (2020), van der Linden et al. (2022), and van den Bos et al. (2024) to solve for optimal trees more effectively. Additionally, Mazumder et al. (2022) apply the Branch-and-Bound method to find globally optimal tree structures. While these approaches improve the global optimality of tree-based models, they do not consider parameter fusion, which is crucial for leveraging shared information across different parts of the model. Moreover, none of these works specifically addresses causal subgroup identification. This gap highlights the need for methods that can efficiently construct globally optimal trees while incorporating parameter fusion constraints to enhance subgroup identification and treatment effect estimation.

2 Problem setup

We consider a setup with n subjects, where the data-generating distribution is denoted by \mathbb{P}_0 , such that $(\mathbf{X}_i, T_i, Y_i) \sim_{i.i.d.} \mathbb{P}_0$ for $i = 1, \dots, n$. Here, $\mathbf{X}_i \in \mathbb{R}^d$ represents the d -dimensional covariates that potentially captures the heterogeneity. T is a binary variable that can be

intervened on, and Y is the outcome of interest.

We assume there exists M^* unknown heterogeneous subpopulations $\mathcal{A}_1^*, \dots, \mathcal{A}_{M^*}^*$ and let $\Pi^* = \{\mathcal{A}_m^*\}_{m=1}^{M^*}$ denote the collection of these subpopulations. Then we model the heterogeneity using the following linear structural equation model:

$$\begin{aligned}
 Y_i &= \sum_{m=1}^{M^*} 1_{(\mathbf{X}_i \in \mathcal{A}_m^*)} \cdot f_m(\mathbf{X}_i, T_i) + \epsilon, \\
 f_m(\mathbf{X}_i, T_i) &= \delta_m^* + \mu_m^* \cdot T_i + \boldsymbol{\alpha}_m^{*\top} \cdot \mathbf{X}_i + \boldsymbol{\beta}_m^{*\top} \cdot T_i \mathbf{X}_i,
 \end{aligned} \tag{1}$$

where ϵ is independent of (T_i, \mathbf{X}_i) with mean 0. This model includes both main effects and treatment-covariate interactions, allowing for flexible characterization of heterogeneity. For notational convenience, we let $\mathbf{Z}_i = [1, T_i, \mathbf{X}_i^\top, T_i \mathbf{X}_i^\top]^\top$ and $\boldsymbol{\gamma}_m^* = (\delta_m^*, \mu_m^*, \boldsymbol{\alpha}_m^{*\top}, \boldsymbol{\beta}_m^{*\top})^\top \in \mathbb{R}^{2d+2}$. In addition, to encourage information sharing between different subgroups, we allow the number of unique values in the vector $\{\gamma_{1j}^*, \dots, \gamma_{M^*j}^*\}$ to be less than M^* .

The above model provides a general framework for gaining deeper insights into studying heterogeneity in clinical trials. By capturing how baseline covariates and their interactions with treatment influence outcomes across subpopulations, it facilitates more interpretable subgroup analyses and supports downstream causal investigations.

3 Methodology

3.1 Fused and globally optimal causal tree to discover heterogeneity

To identify heterogeneous subpopulations and conduct downstream causal analysis of the effects of treatments on the outcome, we aim to estimate the true subgroup partition Π^* and the corresponding parameters $\{\boldsymbol{\gamma}_m^*\}_{m=1}^{M^*}$ in model (1). To efficiently discover informative and interpretable subgroups, we propose estimating Π^* by partitioning the covariate space via a learned hierarchical structure, analogous to recursive partitioning tree-based methods.

To be specific, we formulate the following optimization problem:

$$\begin{aligned} \min_{\{\boldsymbol{\gamma}_m\}_{m=1}^{M(\Pi)}, \Pi \in \mathcal{T}} \sum_{i=1}^n \left\| Y_i - \sum_{m=1}^{M(\Pi)} 1_{(\mathbf{X}_i \in \mathcal{A}_m)} \cdot \boldsymbol{\gamma}_m^\top \mathbf{Z}_i \right\|_2^2, \\ \text{s.t. } \gamma_{l_1, j} = \gamma_{l_2, j}, \text{ for some } l_1 \neq l_2 \text{ and some } j. \end{aligned} \quad (2)$$

where \mathcal{T} denotes the collection of all possible hierarchical partitions and $M(\Pi)$ is the number of subgroups in the partitions Π . The objective function in (2) is designed to facilitate heterogeneous causal discovery, while the parameter fusion constraint enables information sharing across subgroups to maintain statistical efficiency.

The parameter fusion constraint here does not enforce full homogeneity across all leaf nodes but instead allows selective homogeneity across specific covariates. This flexibility accommodates both fully agnostic fusion and fusion guided by prior knowledge. For instance, if a rare genetic variant has sparse representation within certain subgroups, we may enforce parameter fusion on its coefficient to stabilize estimation. By incorporating this constraint, we enhance efficiency for homogeneous effects, improving both subgroup identification accuracy and parameter estimation precision.

The solution to this optimization problem yields the estimated partition $\hat{\Pi} = \{\hat{\mathcal{A}}_m\}_{m=1}^{\hat{M}(\hat{\Pi})}$, where $\hat{M}(\hat{\Pi})$ is the number of identified subgroups, and the corresponding regression parameters $\{\hat{\boldsymbol{\gamma}}_m\}_{m=1}^{\hat{M}(\hat{\Pi})}$ characterize the learned structural relationships within each subgroup.

Challenges: Directly solving the optimization problem in (2) is hard. Existing recursive partitioning tree-based methods employ a greedy top-down approach to obtain a sub-optimal result (See Appendix I). As explained in the introduction, this strategy presents significant limitations in the context of clinical trials with small sample sizes. In such settings, greedy methods lack guarantees of global optimality and are especially prone to generating unstable and inaccurate subgroup partitions. Such inaccurate subgroup discovery can affect downstream clinical interventions in clinical trials. Moreover, the parameter fusion constraints for subgroup information sharing are difficult to implement in the existing tree-based approaches, as they

find different splits in isolation and fail to incorporate a global constraint across different partitions. In response to these challenges, we present a novel formulation of tree-based sample space partition problems using modern mixed-integer optimization (MIO) (See Appendix F for more backgrounds) techniques presented in Algorithm 1. The adoption of MIO offers the additional advantage of seamlessly integrating the tree structure and parameter fusion constraints of Problem (2) into a single unified optimization problem.

3.2 Solving fused optimal causal tree based on mixed integer optimization

In this section, we propose a fused optimal causal tree framework that directly solves the optimization problem in (2), yielding globally optimal subgroup partitions while allowing information sharing across subgroups. We achieve this by reformulating the problem as a mixed-integer optimization problem in Algorithm 1, which can be solved using the state-of-the-art mathematical optimization solver (Gurobi Optimization, LLC, 2024). MIO offers a principled alternative by enabling the global optimization of subgroup partitions under complex structural constraints and parameter fusion constraints. This opens up new opportunities to improve both the accuracy and efficiency of subgroup analyses, particularly in settings with limited samples and partially shared effect structures. Now we present the use of MIO in Algorithm 1 in detail. To save space, we put the detailed explanations of the notations in Appendix G.

MIO neatly represents the tree with binary indicator variables that the algorithm optimizes directly. Let \mathcal{T}_L denote the set of leaf nodes in the hierarchical partition. We reformulate the loss function using binary indicators $\{z_{it'}\}_{i \in [n], t' \in \mathcal{T}_L}$, where $z_{it'} = 1$ if the i -th subject is assigned to leaf node t' , and $z_{it'} = 0$ otherwise. This representation

allows the objective function to be expressed as:

$$L_n(\mathcal{T}_L, \{\boldsymbol{\gamma}_{t'}\}_{t' \in \mathcal{T}_L}) = \sum_{i \in [n]} \left\| Y_i - \sum_{t' \in \mathcal{T}_L} z_{it'} \cdot \boldsymbol{\gamma}_{t'}^\top \mathbf{Z}_i \right\|_2^2.$$

To formulate Π , the subgroup partition that follows a hierarchical tree structure, we introduce several constraints, which can be divided into the following two parts.

MIO seamlessly incorporates subgroup membership constraint. The first part models the subgroup membership of the subjects. The first constraint ensures that each subject i in a leaf node t_0 (where $z_{it_0} = 1$) follows a homogeneous linear regression model. The second constraint ensures that each subject belongs to exactly one leaf node. The third constraint identifies empty leaf nodes ($l_{t'} = 0$) by enforcing $z_{it'} = 0$ for all i . The fourth constraint requires that non-empty leaf nodes ($l_{t'} = 1$) contain at least N_{\min} subjects.

MIO precisely and flexibly represents tree structures. The second set of constraints enforces the hierarchical structure of the partitions. We let \mathcal{T}_B denote the branch nodes that partition the sample space. The first two inequalities define the tree splits using binary vectors $\{\mathbf{a}_m\}_{m \in \mathcal{T}_B}$ and continuous variables $\{b_m\}_{m \in \mathcal{T}_B}$. Subjects in a leaf node t' are characterized by all the splits in the ancestor nodes of t' , with $\mathbf{a}_m^\top \mathbf{X}_i < b_m$ for left branches and $\mathbf{a}_m^\top \mathbf{X}_i \geq b_m$ for right branches. The third and fourth constraints allow branch nodes to remain unsplit ($d_{t'} = 0$) or enforce splits on a single variable for branch nodes that are split ($d_{t'} = 1$). The final constraint ensures the hierarchical structure by preventing a branch node from splitting unless its parent node has already split.

MIO naturally accommodates parameter fusion constraints, enabling effective information sharing across subgroups. In addition to these, we need to incorporate the parameter fusion constraint to facilitate information sharing across subgroups. To add this,

we augment the objective function with an L_0 -fusion penalty $\lambda \sum_{t_1, t_2 \in \mathcal{T}_L, t_1 \neq t_2} r_{jt_1 t_2}$ such that

$$(\gamma_{t_1 j} - \gamma_{t_2 j}) \cdot (1 - r_{jt_1 t_2}) = 0,$$

$$r_{jt_1 t_2} \in \{0, 1\}, \forall j \in [2d + 2], t_1, t_2 \in \mathcal{T}_L \text{ and } t_1 \neq t_2.$$

Here, the parameter λ controls the level of parameter fusion, with larger values encouraging greater homogeneity and smaller values allowing for more heterogeneity. The introduction of this fusion penalty significantly improves sample efficiency by reducing the dimensionality of the parameter space. Importantly, it can alter the learned tree structure (subgroups)—a capability not present in existing tree-based methods.

Tuning parameter selection: To tune the optimal value of λ , we employ the Bayesian Information Criterion (BIC), which is widely used in model selection (Schwarz, 1978). We select λ that minimizes the following BIC expression: $\text{BIC}(\lambda) = n \cdot \log(L_n(\hat{\mathcal{T}}_L, \{\hat{\gamma}_t\}_{t \in \hat{\mathcal{T}}_L})/n) + \text{df}(\lambda) \cdot \log(n)$, where $\text{df}(\lambda) = \sum_{j=1}^{2d+2} \#\{\text{Distinct } \hat{\gamma}_{tj} \text{ for } t \in \hat{\mathcal{T}}_L\}$ is the number of distinct parameters across subgroups. Typically, the choice of λ depends on the sample size n . To eliminate this dependence and simplify the implementation, we normalize the loss function by $\hat{L}(\mathcal{D}_n)$, where $\hat{L}(\mathcal{D}_n)$ is the loss from fitting a single linear regression model to the entire training dataset \mathcal{D}_n . In our implementation, we use a grid search to select the optimal λ by minimizing $\text{BIC}(\lambda)$. Specifically, we compute: $\hat{\lambda}_{BIC} = \min_{\lambda \in \Lambda} \text{BIC}(\lambda)$, Where Λ is the predefined grid of candidate values for λ . We then use the corresponding $\hat{\mathcal{T}}_L, \{\hat{\gamma}_t\}_{t \in \hat{\mathcal{T}}_L}$ for the selected $\hat{\lambda}_{BIC}$ as the final solution.

Algorithm 1: Fused Optimal Causal Tree

Optimization objective:

$$\min_{\Theta \in \Theta} L_n(\mathcal{T}_L, \{\gamma_{t'}\}_{t' \in \mathcal{T}_L}) / \hat{L}(\mathcal{D}_n) + \lambda \cdot \sum_{t_1, t_2 \in \mathcal{T}_L; t_1 \neq t_2} r_{jt_1 t_2}$$

Constraints for the subgroup membership:

$$\begin{aligned} & \left(\sum_{t' \in \mathcal{T}_L} z_{it'} \cdot \gamma_{t'}^\top \mathbf{Z}_i - \gamma_{t_0}^\top \mathbf{Z}_i \right) \cdot z_{it_0} = 0, \forall i \in [n], t_0 \in \mathcal{T}_L; \\ & \sum_{t' \in \mathcal{T}_L} z_{it'} = 1, \quad \forall i \in [n]; \\ & z_{it'} \leq l_{t'}, \quad \forall i \in [n], t' \in \mathcal{T}_L; \\ & \sum_{i=1}^n z_{it'} \geq N_{\min} l_{t'}, \quad \forall t' \in \mathcal{T}_L; \\ & z_{it'}, l_{t'} \in \{0, 1\}, \quad \forall i \in [n], t' \in \mathcal{T}_L; \end{aligned}$$

Constraints for the tree structure:

$$\begin{aligned} & \mathbf{a}_m^\top \mathbf{X}_i \geq b_m - (1 - z_{it'}), \quad \forall i \in [n], t' \in \mathcal{T}_L, m \in \mathcal{R}(t'); \\ & \mathbf{a}_m^\top \mathbf{X}_i < b_m + (1 - z_{it'}), \quad \forall i \in [n], t' \in \mathcal{T}_L, m \in \mathcal{L}(t'); \\ & \sum_{k=1}^d a_{t'k} = d_{t'}, \quad \forall t' \in \mathcal{T}_B; \\ & 0 \leq b_{t'} \leq d_{t'}, \quad \forall t' \in \mathcal{T}_B; \\ & d_{t'} \leq d_{\mathbf{p}(t')}, \quad \forall t' \in \mathcal{T}_B \setminus \{\text{root}\}; \\ & a_{t'k}, d_{t'} \in \{0, 1\}, \quad \forall k \in [d], t' \in \mathcal{T}_B; \end{aligned}$$

Fusion constraints for information sharing:

$$\begin{aligned} & (\gamma_{t_1 j} - \gamma_{t_2 j})(1 - r_{jt_1 t_2}) = 0, \quad \forall t_1, t_2 \in \mathcal{T}_L, \text{ and } t_1 \neq t_2; \\ & r_{jt_1 t_2} \in \{0, 1\}, \quad \forall j \in [2d + 2], t_1, t_2 \in \mathcal{T}_L, \text{ and } t_1 \neq t_2. \end{aligned}$$

3.3 Causal analysis with fused optimal causal tree

A downstream goal in the subgroup analysis is to estimate the subgroup average treatment effect (SATE). Under standard causal assumptions and model (1) (See Appendix H for more details), the SATE for any subject i can be given by

$$\tau(\mathbf{X}_i, \Pi^*) = \sum_{m=1}^{M^*} 1_{(\mathbf{X}_i \in \mathcal{A}_m^*)} \cdot (\mu_m^* + \boldsymbol{\beta}_m^{*T} \bar{\mathbf{X}}_m).$$

where $\bar{\mathbf{X}}_m = \mathbb{E}[\mathbf{X}_i | \mathbf{X}_i \in \mathcal{A}_m^*]$. The solution to optimization problem (2) yields a natural estimator of $\tau(\mathbf{X}_i, \Pi^*)$:

$$\hat{\tau}(\mathbf{X}_i, \hat{\Pi}) = \sum_{m=1}^{\hat{M}(\hat{\Pi})} 1_{(\mathbf{X}_i \in \hat{\mathcal{A}}_m)} \cdot (\hat{\mu}_m + \hat{\boldsymbol{\beta}}_m^\top \hat{\bar{\mathbf{X}}}_m).$$

where $\hat{\bar{\mathbf{X}}}_m$ is the sample average of \mathbf{X}_i in $\hat{\mathcal{A}}_m$. To provide confidence intervals for $\tau(\mathbf{X}_i, \Pi^*)$ and enable valid statistical inference, we fix the subgroups and parameter fusion structure obtained from Algorithm 1 and generate bootstrap samples B times. For each bootstrap sample, we run the linear regression model with the parameter fusion pattern learned from the original sample, and then use the estimated coefficients and subgroup sample averages to estimate $\tau(\mathbf{X}_i, \Pi^*)$. Then we use the quantiles of these B estimators to construct the confidence intervals.

To ensure good estimation performance of $\hat{\tau}(X_i, \hat{\Pi})$ on $\tau(X_i, \Pi)$, we need to ensure (1) subgroup identification accuracy: whether $\hat{\Pi}$ accurately recovers Π^* , (2) parameter estimation efficiency: whether $\hat{\boldsymbol{\gamma}}_m$ efficiently estimates $\boldsymbol{\gamma}_m$. As discussed in Section 1.2, our proposed fused optimal causal tree improves performance on both points compared to existing tree-based methods, leading to improved statistical efficiency. These advantages are demonstrated in the simulation results presented in Section 5. In addition, a simple example is provided in Appendix J to help illustrate this.

4 Theoretical Investigation

In this section, we present a rigorous theoretical investigation of risk bounds for the optimal tree and greedy tree. We first introduce some notation.

4.1 Notations

We consider the following non-parametric regression model:

$$Y = f^*(\mathbf{Z}) + \epsilon,$$

where $\epsilon = Y - \mathbb{E}[y|\mathbf{Z}] = y - f^*(\mathbf{Z})$ is a sub-gaussian noise in the sense that there exists $\sigma^2 > 0$ such that for all $u \geq 0$, $\mathbb{P}(|\epsilon| \geq u) \leq \exp(-u/(2\sigma^2))$.

In our regression model (1), we treat $\mathbf{Z} = [1, T, \mathbf{X}^\top, T\mathbf{X}^\top]^\top$, but the results in this section hold for more general forms of $\mathbf{Z} \in \mathbb{R}^p$. To evaluate the performance of a given tree regression approach, we use the following prediction risk measure:

$$\|f - f^*\|_2^2 = \mathbb{E}_{\mathbf{Z}} [(f^*(\mathbf{Z}) - f(\mathbf{Z}))^2].$$

We consider a function class of h -way interaction regression functions

$$\mathcal{F}^h := \{f(\mathbf{Z}) | f(\mathbf{Z}) := \sum_{j_1} f_{j_1}(Z_{j_1}) + \dots + \sum_{j_1 < j_2 < \dots < j_h} f_{j_1, j_2, \dots, j_h}(Z_{j_1}, Z_{j_2}, \dots, Z_{j_h})\},$$

and define the norm $\|f\|_\infty = \sup_{\mathbf{Z} \in \mathcal{Z}} |f(\mathbf{Z})|$.

In addition, given a tree $T_K = \{\{\hat{\mathcal{A}}_j\}_{j=1}^{M(T_K)}, \{\hat{\gamma}_j\}_{j=1}^{M(T_K)}\}$, we denote the estimator of f^* as

$$\hat{f}(T_K)(\mathbf{Z}) = \sum_{j=1}^{M(T_K)} 1_{(\mathbf{Z} \in \hat{\mathcal{A}}_j)} (\hat{\gamma}_j)^T \mathbf{Z}.$$

Where $\{\hat{\mathcal{A}}_j\}_{j=1}^{M(T_K)}$ is the collection of its leaf nodes and $\{\hat{\gamma}_j\}_{j=1}^{M(T_K)} \in \mathbb{R}^p$ are the coefficient

estimates obtained by fitting a linear model in each leaf node. We also let $\mathbb{E}_{\mathcal{D}_n}[\cdot]$ denote the expectation taken with respect to the training sample \mathcal{D}_n .

4.2 Theoretical results

Now we present the out-of-sample risk bounds for both the optimal tree and greedy CART algorithm.

4.2.1 Risk bound for optimal tree

Assumption 4.1. Let $\mathbf{Z} \in [0, 1]^p$ and $f^* \in \mathcal{F}^h$ is a piece-wise linear function induced by a depth K tree $T_K^* = \{\{\mathcal{A}_j^*\}_{j=1}^{M(T_K^*)}, \{\boldsymbol{\gamma}_j^*\}_{j=1}^{M(T_K^*)}\}$ in the sense that

$$f^*(\mathbf{Z}) = \sum_{j=1}^{M(T_K^*)} 1_{\{\mathbf{Z} \in \mathcal{A}_j^*\}} \boldsymbol{\gamma}_j^{*T} \mathbf{Z}.$$

In addition, the l_1 -norm of the coefficient vectors in each piece of f^* are uniformly bounded by B in the sense that

$$\|\boldsymbol{\gamma}_j\|_1 = \sum_{k \in [p]} |\gamma_{jk}| \leq B, \quad \forall j = 1, \dots, M(T_K^*).$$

Theorem 4.2 (Risk bound for optimal tree). *If f^* satisfies Assumption 4.1, then under the sub-gaussian condition on ϵ , we have*

$$\mathbb{E}_{\mathcal{D}_n} \left(\left\| \hat{f}(T_K^{\text{OT}}) - f^* \right\|_2^2 \right) \leq C_1 \frac{2^K \log^2(N) ((p+1) \log(N) + \log(p))}{N}.$$

where T_K^{OT} is a depth K optimal tree obtained by Algorithm 1, C_1 is a positive constant depending only on B in Assumption 4.1 and σ^2 .

When the underlying true subgroup partition is known, the minimax risk lower bound for fitting a piecewise linear function with 2^K pieces is $O(2^K p \sigma^2 / N)$. Theorem 4.2 implies that,

if the true underlying regression function is a piecewise linear function induced by a depth K tree, then we can show the estimator based on the optimal regression tree approach can achieve near-optimal convergence rate with an additional logarithmic factor.

4.2.2 Risk bound for CART

To present the risk bound of CART, we need an additional technical assumption, which is used to handle the challenges in theoretical analysis caused by the greedy nature of CART. To save space, we provide this assumption and some comments in Appendix A.

Theorem 4.3 (Risk bound for CART). *Let T_K^{CART} be a depth K tree obtained by CART with the splitting criteria in (4). If f^* and T_K satisfy the Assumption 4.1 and Assumption A.1, then under the sub-gaussian condition on ϵ , we have*

$$\mathbb{E}_{\mathcal{D}_n} \left(\left\| \hat{f}(T_K^{\text{CART}}) - f^* \right\|_2^2 \right) \leq \frac{C_0 h}{K + 2h + 1} + C_1 \frac{2^K \log^2(N) ((p + 1) \log(N) + \log(p))}{N}.$$

where C_0 is a positive constant depends on f^* , C_1 is a positive constant that depends only on B in Assumption 1 and σ^2 .

Compared to the risk bound of the optimal tree, the risk bound of CART depends on an additional term $C_0 \cdot h / (K + 2h + 1)$. This means that CART needs depth $K \rightarrow \infty$ to consistently estimate the regression function f^* . Furthermore, this risk bound is derived under an additional stringent assumption (Assumption A.1), which is often hard to verify in practice. The condition $K \rightarrow \infty$ required to ensure the consistency of CART inherently exacerbates overfitting, as increasing the tree depth introduces more parameters to estimate. In contrast, optimal regression trees do not rely on this condition for consistency, allowing for fewer parameters and mitigating overfitting. This further shows the superiority of optimal tree over greedy CART algorithm.

5 Simulation

5.1 Simulation Setup

We consider the following data-generating process:

$$T \sim \text{Bernoulli}(p); \quad X_1 \sim \mathcal{N}(0, 1); \quad \mathbf{X}_{-1} \sim \mathcal{N}(\mathbf{0}, \boldsymbol{\Sigma});$$

$$Y = \sum_{m=1}^{M^*} 1_{(\mathbf{X} \in \mathcal{A}_m^*)} (\delta_m + \mu_m T + \boldsymbol{\alpha}_m^\top \mathbf{X} + \boldsymbol{\beta}_m^\top T \mathbf{X}) + \epsilon.$$

where \mathbf{X}_{-1} is the vector $\mathbf{X} \in \mathbb{R}^d$ without the first component. $\boldsymbol{\Sigma}$ is a matrix with 1s on the diagonal and ρ in the off-diagonal entries. Here ρ controls the correlation between some spurious split variables and the true split variable that determines the subgroup partitions. When ρ is larger, it will be more difficult to identify the underlying subgroup partitions. Another two parameters p and d control the balance level of the treatment and control groups and the dimension of covariates \mathbf{X} . We test the performance of different methods for $\rho \in \{0.7, 0.8\}$, $p = 0.3$, and $d = 3$ in the main manuscript and provide more simulations for other scenarios with different parameters in Appendix E.

We set the number of subgroups $M^* = 4$ such that $\mathcal{A}_1^* = \{\mathbf{X} | X_1 < 0, X_2 < 0\}$, $\mathcal{A}_2^* = \{\mathbf{X} | X_1 < 0, X_2 \geq 0\}$, $\mathcal{A}_3^* = \{\mathbf{X} | X_1 \geq 0, X_2 < 0\}$ and $\mathcal{A}_4^* = \{\mathbf{X} | X_1 \geq 0, X_2 \geq 0\}$. We provide the parameter specifications and the exact expressions of SATE, $\tau(\mathbf{x}, \Pi^*, \rho)$, in Appendix D.

5.2 Methods

Causal Tree by CART (CT-CART): We implement Breiman’s original regression tree (CART) with a linear regression model in each leaf node and the splitting criteria discussed in (4) in the Appendix.

Optimal Causal Tree without Fusion (OCT): The optimal causal tree is implemented by Algorithm 1 without the fusion constraint. In other words, we set $\lambda = 0$. We use Gurobi

to solve this with 1 hour limit.

Fused Optimal Causal Tree (FOCT): The fused optimal causal tree is implemented by Algorithm 1 with fusion constraints. We tune the λ in the grid $\Lambda = \{1/10000 * i | i = 1, \dots, 15\}$ and use BIC to choose the optimal λ . For each λ , we use Gurobi to solve this optimization problem with 1 hour limit.

For all these three methods, we set the tree depth as 2 and the minimal leaf size as $N_{min} = 1$. The collection of leaf nodes can serve as the identified subgroups and be used to estimate $\tau(\mathbf{x}, \Pi^*, \rho)$ for any given observation $\mathbf{X} = \mathbf{x}$, which will be

$$\hat{\tau}(\mathbf{x}, \hat{\Pi}^{\text{me}}, \mathcal{D}_n) = \sum_{m=1}^{\hat{M}^{\text{me}}} 1_{(\mathbf{x} \in \hat{\mathcal{A}}_m^{\text{me}})} \cdot (\hat{\mu}_m^{\text{me}} + (\hat{\beta}_m^{\text{me}})^\top \hat{\mathbf{X}}_m^{\text{me}}).$$

where $\text{me} \in \{\text{CT-CART}, \text{OCT}, \text{FOCT}\}$ indicates the method we use. $\hat{\Pi}^{\text{me}} = \{\hat{\mathcal{A}}_m^{\text{me}}\}_{m=1}^{\hat{M}^{\text{me}}}$ is the collection of leaf nodes for a given method. $\hat{\mu}_m^{\text{me}}$ and $\hat{\beta}_m^{\text{me}}$ are the corresponding estimates in leaf node $\hat{\mathcal{A}}_m^{\text{me}}$ and $\hat{\mathbf{X}}_m^{\text{me}}$ is the sample average of \mathbf{X} in $\hat{\mathcal{A}}_m^{\text{me}}$. All of them are estimated by training data \mathcal{D}_n .

5.3 Performance metrics

We run 100 Monte Carlo simulations with each using $n_{\text{train}} = 200$ training samples from the data-generating process in Section 5.1, and compare three different performance metrics.

Subgroup identification accuracy: We summarize the number of times that we identify the correct tree structures: depth 2 trees with the split variable in the root node is X_1 (X_2), followed by the split variable X_2 (X_1) in both its left and right child nodes.

SATE estimation precision: The precision of SATE $\tau(\mathbf{x}, \Pi^*, \rho)$ estimates is evaluated by using the following mean squared error (MSE) metric:

$$\frac{1}{n_{\text{test}}} \sum_{i=1}^{n_{\text{test}}} (\hat{\tau}(\mathbf{X}_i, \hat{\Pi}^{\text{me}}, \mathcal{D}_n) - \tau(\mathbf{X}_i, \Pi^*, \rho))^2.$$

Out-of-sample risk: We also evaluate out-of-sample risk, which is the average of the squared differences between predicted values and actual values on test samples. The out-of-sample risk is evaluated on test sample by

$$\frac{1}{n_{\text{test}}} \sum_{i=1}^{n_{\text{test}}} (\hat{f}(\mathbf{Z}_i, \hat{T}^{\text{me}}, \mathcal{D}_n) - f^*(\mathbf{Z}_i))^2.$$

Here \hat{T}^{me} is the tree found by method $\text{me} \in \{\text{CT-CART}, \text{OCT}, \text{FOCT}\}$. In addition, $\hat{f}(\mathbf{Z}_i, \hat{T}^{\text{me}}, \mathcal{D}_n)$ is estimated model with tree \hat{T}^{me} and $f^*(\mathbf{Z}_i)$ is the true mean under model (1).

For the latter two metrics, we use $n_{\text{test}} = 2000$ test samples generated from the same data-generating process to evaluate and compare the performance of different methods.

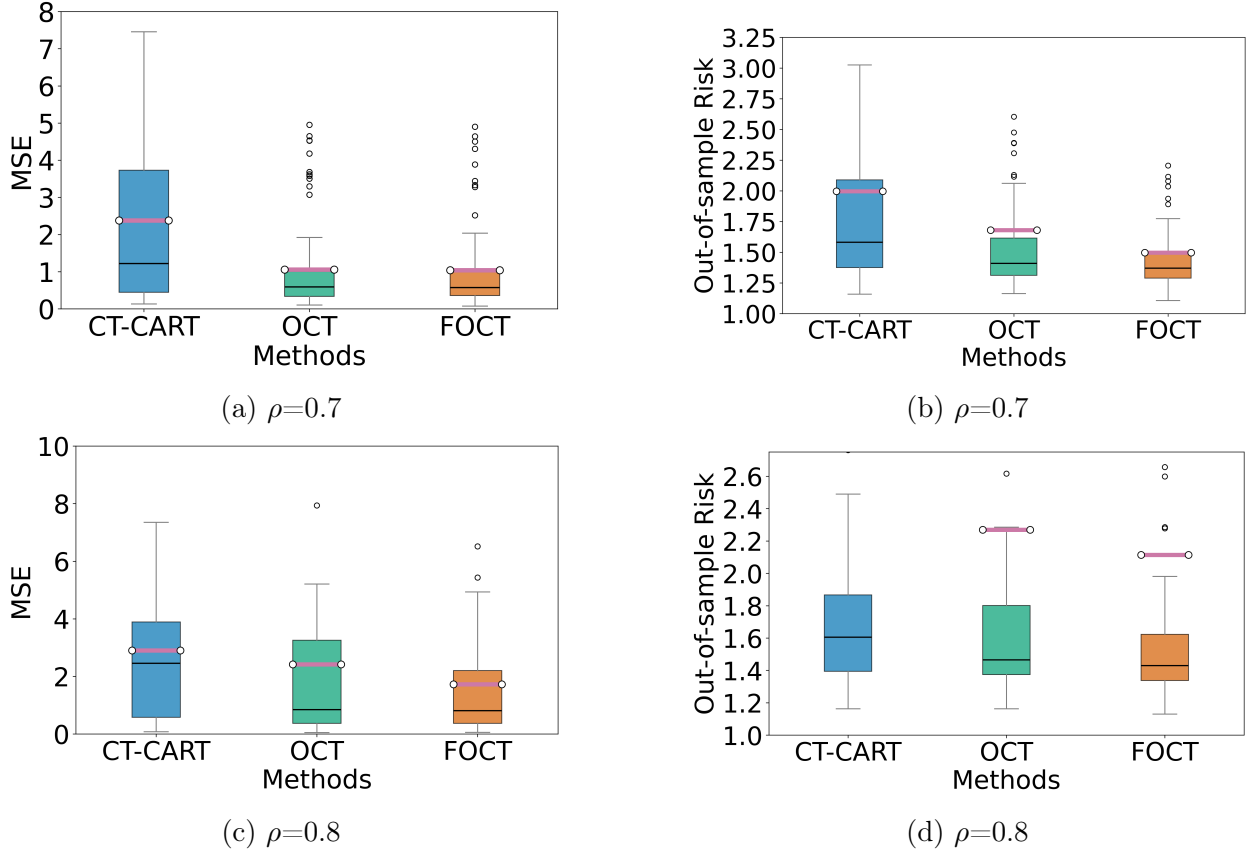


Figure 1: Boxplot of mean square error (MSE) of SATE estimation and out-of-sample risk for different methods with $\rho \in \{0.7, 0.8\}$ across 100 Monte Carlo simulations. The purple line is the mean of MSE (or out-of-sample risk) across 100 Monte Carlo simulations for each method. The purple line for CT-CART in Figure 1d is above 2.7.

5.4 Results

When $\rho = 0.8$, FOCT more frequently recovers the correct tree structure (67 times) than OCT (54 times) and CT-CART (39 times), demonstrating the benefit of fusion constraints in improving subgroup partition accuracy by reducing overfitting and avoiding spurious splits like X_3 . With a smaller $\rho = 0.7$, FOCT (81 times) and OCT (78 times) still outperform CT-CART (51 times), though the gap between FOCT and OCT narrows. This is expected, as stronger signals (smaller ρ) reduce overfitting, lessening the impact of the fusion constraint. Figures 1a and 1b show that when $\rho = 0.7$, both FOCT and OCT achieve lower MSE in SATE estimation and lower out-of-sample risk than CT-CART, with FOCT offering slightly

more stable performance. When $\rho = 0.8$, identifying the true model becomes harder, and the fusion constraint plays a larger role in preventing overfitting and improving both subgroup recovery and estimation efficiency (Figures 1c and 1d).

6 Case Study

6.1 Data

We applied CT-CART, OCT, and FOCT to a dataset with black participants enrolled in the Health and Aging Brain Study–Health Disparities (HABS-HD). After excluding observations with missing data, the analytic sample comprised 237 individuals. The small size of this dataset underscores the necessity for statistically efficient subgroup discovery methods.

We chose covariates that potentially captures the AD heterogeneity, including, for example, sex, the apolipoprotein E2 (APOE2) allele, the apolipoprotein E4 (APOE4) allele, total years of education (Edu), age, tau accumulation in the entorhinal cortex (Tau_1), and tau accumulation in the neocortex (Tau_2). All included covariates have been linked to heterogeneity in AD pathologies: Female sex is associated with faster tau accumulation in vulnerable brain regions (Coughlan et al., 2025). APOE2 provides protection by reducing amyloid and tau burden (Kim et al., 2022), while APOE4 exacerbates pathology through increased amyloid- β deposition, tau spread, and neuroinflammation (Fernández-Calle et al., 2022). Higher education or cognitive reserve is linked to slower decline at equivalent pathology levels (Cody et al., 2024). Age is the strongest AD risk factor, with incidence rising sharply after 65 (Guerreiro and Bras, 2015). Tau accumulation in the entorhinal cortex predicts early memory loss (Cody et al., 2024), and neocortical tau is a strong predictor of dementia progression (Sperling et al., 2024).

For the treatment variable T , we assign individuals with $A\beta \geq 10$ to the group $T = 1$. Those with $A\beta < 10$ are assigned to the group $T = 0$. The outcome of interest, Y , is the Mini-Mental State Examination (MMSE) score, a widely used clinical measure of cognitive

function for AD patients. Demographic characteristics of the analytic sample are summarized in Supplemental Table 1 in the Appendix.

6.2 Implementation details

We standardized all variables prior to analysis and applied our fused optimal causal tree with a maximum depth of 2 to the dataset. To select the tuning parameter for the fusion penalty, we generated a grid of 50 values evenly spaced over the interval $[0, 0.005]$. For each candidate value of λ , we used Gurobi to solve the optimization problem, imposing a one-hour time limit per run. The optimal λ was selected based on BIC. In addition to identifying subgroups, the fused optimal causal tree reveals parameter fusion patterns, indicating which covariates exhibit homogeneous effects across some or all subgroups. Leveraging these identified fusion structures, we refitted a regression model with pooled coefficients and reported the estimated regression coefficients and their corresponding p-values in Supplemental Table 2. We also reported the confidence intervals of coefficients in Figure 3. For SATE, we use the bootstrap method in Section 3.3 with $B = 1000$ to construct confidence intervals. We also compared the results of the other two methods, CT-CART and OCT, with our FOCT.

6.3 Results

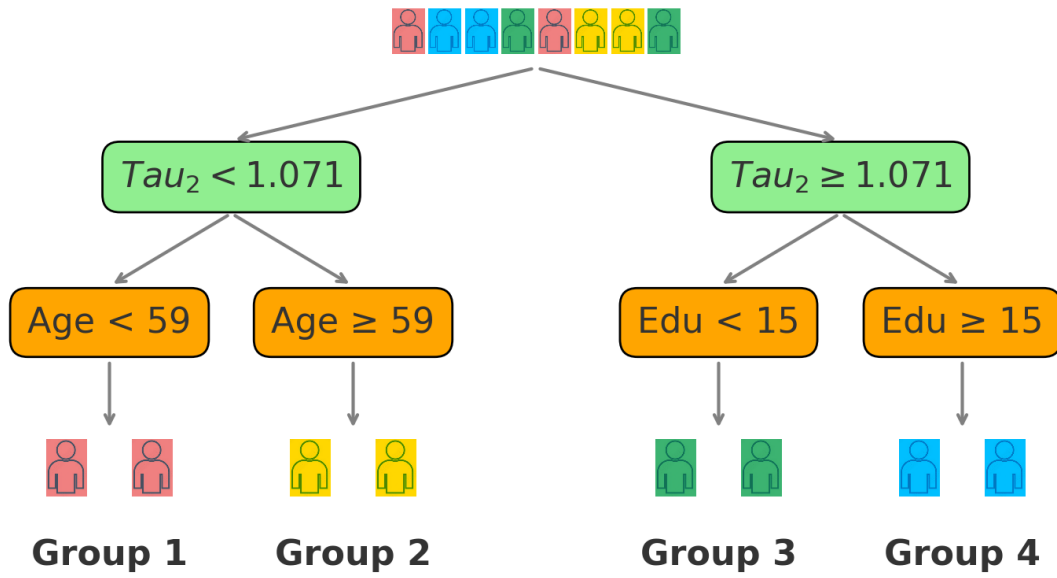
The subgroups identified by FOCT are shown in Figure 2a, defined by neocortical tau levels (Tau_2), education (Edu), and age. As seen in Figure 2b, Group 3—individuals with low education ($Edu < 15$) and high neocortical tau ($Tau_2 \geq 1.071$)—shows a significant benefit from $A\beta$ -lowering treatment, with improved MMSE scores (Negative values in Figure 2b reflect cognitive improvement as $A\beta$ levels decrease). This suggests that individuals in Group 3 may particularly benefit from $A\beta$ -targeting therapies and should receive special attention in downstream AD trials. Figure 3 provides further insights into AD pathophysiology across subgroups. It reveals that age and education are strongly associated with MMSE: MMSE scores decline with age and increase with education. Notably, the positive effect of education

on MMSE is more pronounced in Group 3, indicating a stronger protective role of cognitive reserve among individuals with low education and high tau burden. Additionally, tau accumulation in the neocortex (Tau_2) is significantly associated with MMSE both through its main effect and its interaction with treatment, with Group 3 showing the steepest decline in cognitive performance under high tau levels for $A\beta$ -positive individuals.

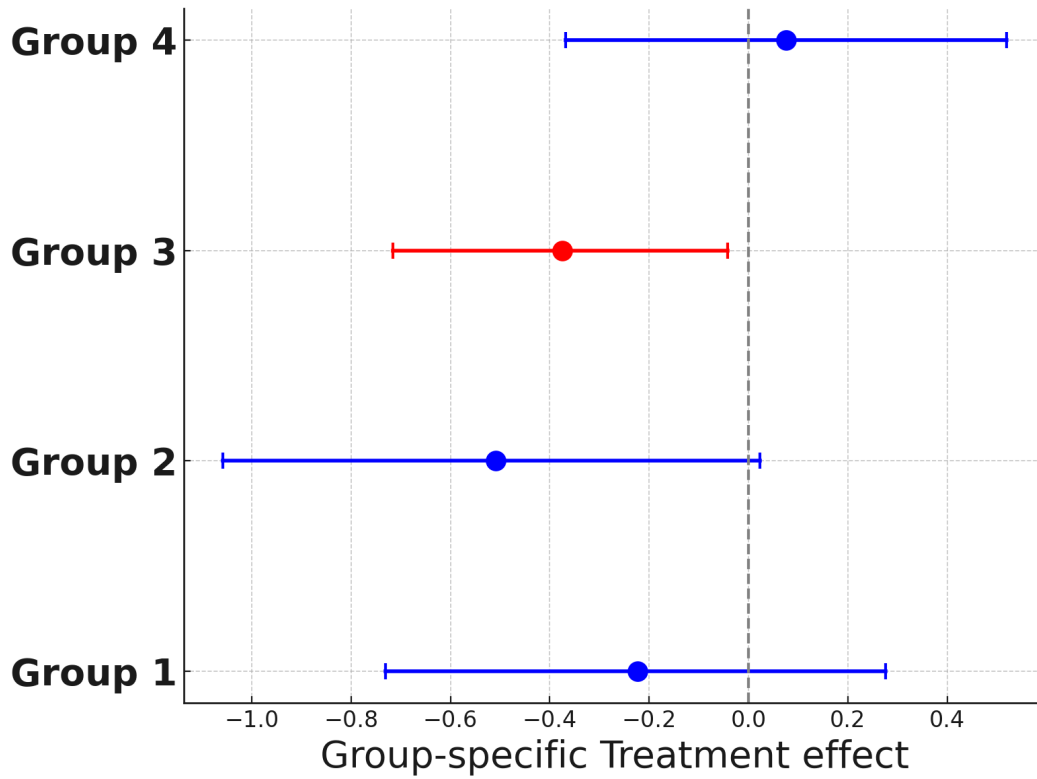
The identified subgroups by CT-CART and OCT are similar—but not identical—to the subgroups identified by FOCT (Figure 4a). However, without the parameter fusion constraint to mitigate overfitting, CT-CART and OCT fail to produce interpretable coefficient estimates for the effects of covariates on the outcome. In particular, for Group 2, both methods estimate a statistically significant positive effect of the interaction between treatment and APOE4 status on MMSE scores—contradicting well-established findings in the AD literature that APOE4 carriage is associated with cognitive decline (Supplemental Table 4). Similarly, these two methods report a statistically significant negative effect of the interaction between treatment and APOE2, despite APOE2 being widely recognized as a protective allele in AD (Supplemental Table 4). Furthermore, both CT-CART and OCT estimate a negative and statistically significant SATE of lowering $A\beta$ on MMSE for Group 2. The bootstrap confidence intervals for SATEs under these methods are also substantially wider, reflecting a general loss of statistical efficiency compared to our FOCT approach (Figure 4b).

7 Discussion

In this paper, we introduce a novel, efficient causal tree approach for subgroup analysis. Unlike existing tree-based methods, our approach identifies optimal subgroup partitions and enhances estimation power by incorporating a fusion constraint that accounts for the global structure of the data. We provide both theoretical analyses and empirical studies to demonstrate the superior performance of our method in terms of subgroup identification accuracy and causal effect estimation. We further illustrate its utility through a case study that yields



(a) Subgroups identified by FOCT.



(b) Group-specific treatment effects of $A\beta$ intervention on MMSE with 90% confidence intervals. Red segment indicate significant effects.

Figure 2: Summary of findings by FOCT: HABS-HD case study on black individuals.

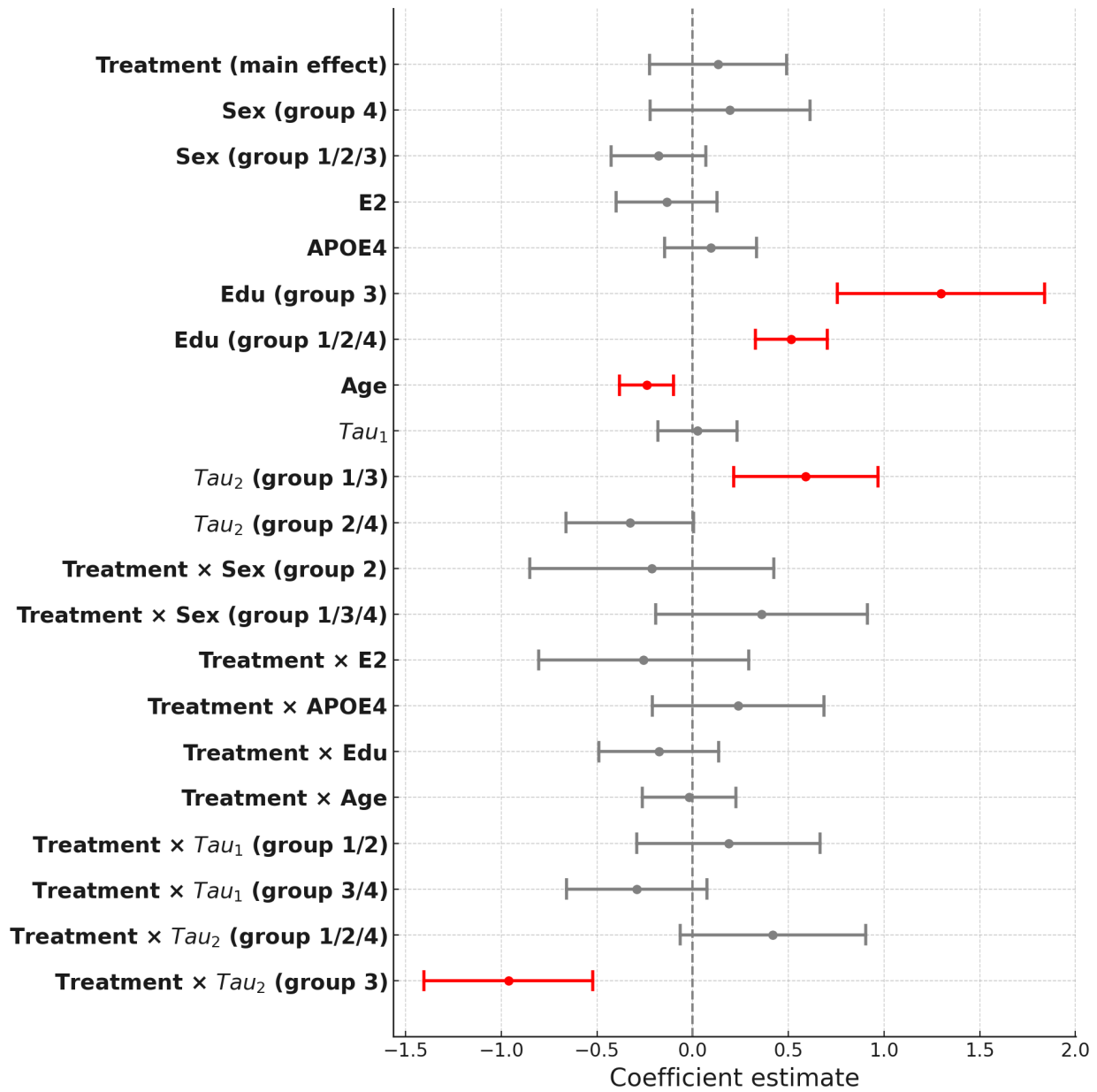
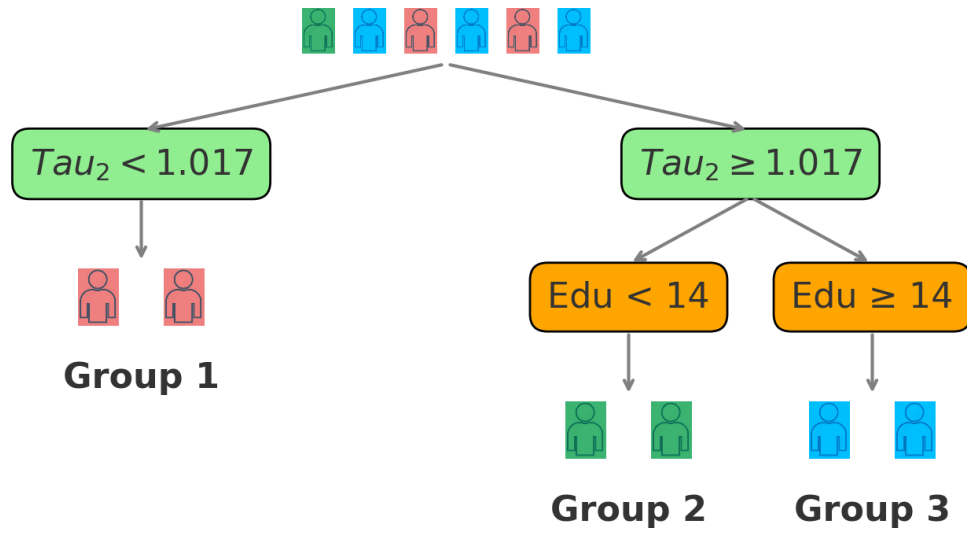
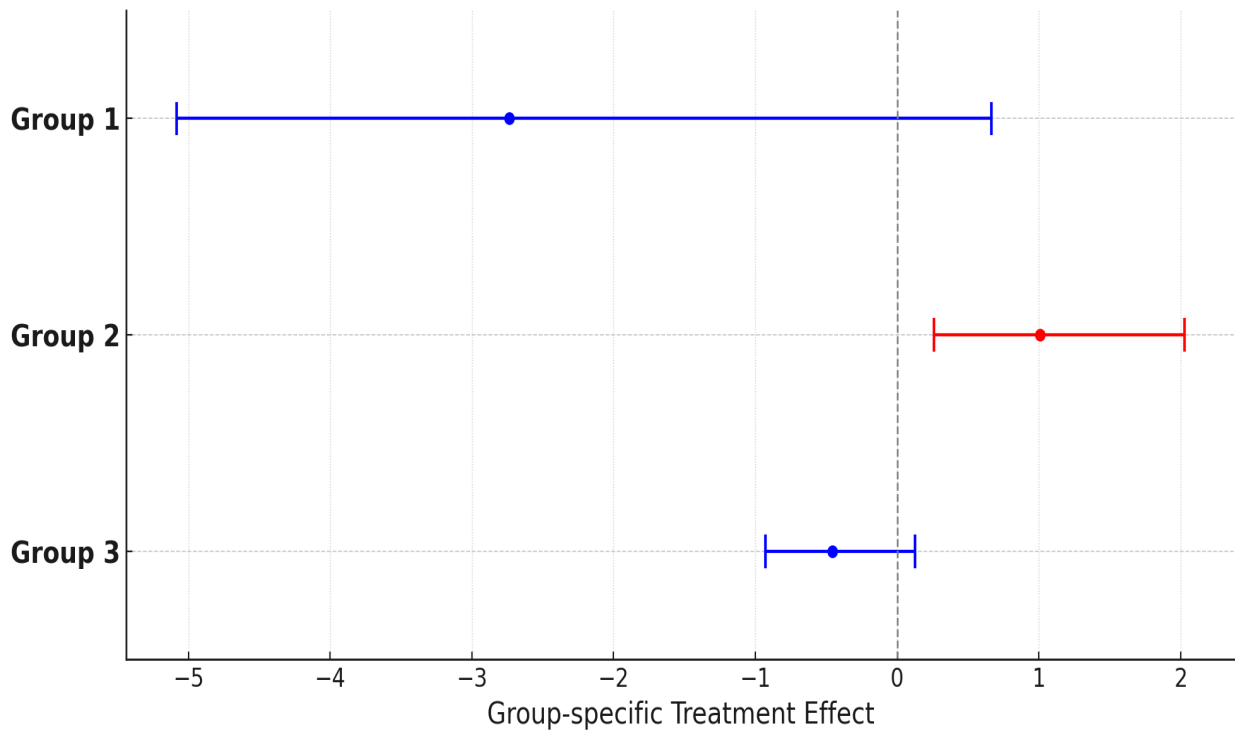


Figure 3: Coefficient estimates in the regression model with parameter fusion pattern learned by FOCT with 90% confidence intervals. Red segments indicate statistically significant coefficients; grey segments indicate non-significant ones.



(a) Subgroups identified by OCT/CT-CART.



(b) Group-specific treatment effects of $A\beta$ intervention on MMSE with 90% confidence intervals. Red segment indicate significant effects.

Figure 4: Summary of findings by OCT/CT-CART: HABS-HD case study on black individuals.

interpretable clinical insights. Future directions include developing a more computationally efficient algorithm to alleviate the burden of solving the underlying mixed-integer optimization problem and extending the method to longitudinal data, which is essential for robust subgroup analysis (Wei et al., 2020).

References

- Athey, S. and Imbens, G. (2016). Recursive partitioning for heterogeneous causal effects. *Proceedings of the National Academy of Sciences*, 113(27):7353–7360.
- Bertsimas, D. and Dunn, J. (2017). Optimal classification trees. *Machine Learning*, 106:1039–1082.
- Chatterjee, S. and Goswami, S. (2021). Adaptive estimation of multivariate piecewise polynomials and bounded variation functions by optimal decision trees. *The Annals of Statistics*, 49(5):2531–2551.
- Cody, K. A., Langhough, R. E., Zammit, M. D., Clark, L., Chin, N., Christian, B. T., Betthausen, T. J., and Johnson, S. C. (2024). Characterizing brain tau and cognitive decline along the amyloid timeline in alzheimer’s disease. *Brain*, 147(6):2144–2157.
- Coughlan, G. T., Klinger, H. M., Boyle, R., Betthausen, T. J., Binette, A. P., Christenson, L., Chadwick, T., Hansson, O., Harrison, T. M., Healy, B., et al. (2025). Sex differences in longitudinal tau-pet in preclinical alzheimer disease: A meta-analysis. *JAMA neurology*, 82(4):364–375.
- Demirović, E., Lukina, A., Hebrard, E., Chan, J., Bailey, J., Leckie, C., Ramamohanarao, K., and Stuckey, P. J. (2022). Murtree: Optimal decision trees via dynamic programming and search. *Journal of Machine Learning Research*, 23(26):1–47.
- Fernández-Calle, R., Konings, S. C., Frontiñán-Rubio, J., García-Revilla, J., Camprubí-Ferrer,

- L., Svensson, M., Martinson, I., Boza-Serrano, A., Venero, J. L., Nielsen, H. M., et al. (2022). Apoe in the bullseye of neurodegenerative diseases: impact of the apoe genotype in alzheimer’s disease pathology and brain diseases. *Molecular neurodegeneration*, 17(1):62.
- Guerreiro, R. and Bras, J. (2015). The age factor in alzheimer’s disease. *Genome medicine*, 7:1–3.
- Gurobi Optimization, LLC (2024). Gurobi Optimizer Reference Manual.
- Györfi, L., Kohler, M., Krzyzak, A., and Walk, H. (2006). *A distribution-free theory of nonparametric regression*. Springer Science & Business Media.
- Hahn, P., Murray, J. S., and Carvalho, C. M. (2020). Bayesian regression tree models for causal inference: Regularization, confounding, and heterogeneous effects. *Bayesian Analysis*, 15(3):965–1056.
- Hill, J. L. (2011). Bayesian nonparametric modeling for causal inference. *Journal of Computational and Graphical Statistics*, 20(1):217–240.
- Kim, H., Devanand, D. P., Carlson, S., and Goldberg, T. E. (2022). Apolipoprotein e genotype e2: Neuroprotection and its limits. *Frontiers in Aging Neuroscience*, 14:919712.
- Klusowski, J. M. and Tian, P. M. (2024). Large scale prediction with decision trees. *Journal of the American Statistical Association*, 119(545):525–537.
- Lin, J., Zhong, C., Hu, D., Rudin, C., and Seltzer, M. (2020). Generalized and scalable optimal sparse decision trees. In *International Conference on Machine Learning*, pages 6150–6160. PMLR.
- Loh, W.-Y., He, X., and Man, M. (2015). A regression tree approach to identifying subgroups with differential treatment effects. *Statistics in medicine*, 34(11):1818–1833.

- Mazumder, R., Meng, X., and Wang, H. (2022). Quant-bnb: A scalable branch-and-bound method for optimal decision trees with continuous features. In *International Conference on Machine Learning*, pages 15255–15277. PMLR.
- Rubin, D. B. (2005). Causal inference using potential outcomes: Design, modeling, decisions. *Journal of the American Statistical Association*, 100(469):322–331.
- Schwarz, G. (1978). Estimating the dimension of a model. *The annals of statistics*, pages 461–464.
- Shen, J. and He, X. (2015). Inference for subgroup analysis with a structured logistic-normal mixture model. *Journal of the American Statistical Association*, 110(509):303–312.
- Sims, J. R., Zimmer, J. A., Evans, C. D., Lu, M., Ardayfio, P., Sparks, J., Wessels, A. M., Shcherbinin, S., Wang, H., Nery, E. S. M., et al. (2023). Donanemab in early symptomatic alzheimer disease: the trailblazer-alz 2 randomized clinical trial. *Jama*, 330(6):512–527.
- Sperling, R. A., Donohue, M., Rissman, R., Johnson, K., Rentz, D., Grill, J., Heidebrink, J., Jenkins, C., Jimenez-Maggiora, G., Langford, O., et al. (2024). Amyloid and tau prediction of cognitive and functional decline in unimpaired older individuals: longitudinal data from the a4 and learn studies. *The Journal of Prevention of Alzheimer’s Disease*, 11(4):802–813.
- Su, X., Tsai, C.-L., Wang, H., Nickerson, D. M., and Li, B. (2009). Subgroup analysis via recursive partitioning. *Journal of Machine Learning Research*, 10(Feb):141–158.
- Tan, Y. S., Agarwal, A., and Yu, B. (2022). A cautionary tale on fitting decision trees to data from additive models: generalization lower bounds. In *International Conference on Artificial Intelligence and Statistics*, pages 9663–9685. PMLR.
- Tian, L., Alizadeh, A. A., Gentles, A. J., and Tibshirani, R. (2014). A simple method for estimating interactions between a treatment and a large number of covariates. *Journal of the American Statistical Association*, 109(508):1517–1532.

- Ting, A. and Linero, A. R. (2023). Estimating heterogeneous causal mediation effects with bayesian decision tree ensembles. *arXiv preprint arXiv:2303.01620*.
- van den Bos, M., van der Linden, J. G. M., and Demirović, E. (2024). Piecewise constant and linear regression trees: An optimal dynamic programming approach. In *Forty-first International Conference on Machine Learning*.
- van der Linden, J., de Weerdt, M., and Demirović, E. (2022). Fair and optimal decision trees: A dynamic programming approach. *Advances in Neural Information Processing Systems*, 35:38899–38911.
- Van Dyck, C. H., Swanson, C. J., Aisen, P., Bateman, R. J., Chen, C., Gee, M., Kanekiyo, M., Li, D., Reyderman, L., Cohen, S., et al. (2023). Lecanemab in early alzheimer’s disease. *New England Journal of Medicine*, 388(1):9–21.
- Wager, S. and Athey, S. (2018). Estimation and inference of heterogeneous treatment effects using random forests. *Journal of the American Statistical Association*, 113(523):1228–1242.
- Wei, Y., Liu, L., Su, X., Zhao, L., and Jiang, H. (2020). Precision medicine: Subgroup identification in longitudinal trajectories. *Statistical methods in medical research*, 29(9):2603–2616.
- Xue, F., Tang, X., Kim, G., Koenen, K. C., Martin, C. L., Galea, S., Wildman, D., Uddin, M., and Qu, A. (2022). Heterogeneous mediation analysis on epigenomic ptsd and traumatic stress in a predominantly african american cohort. *Journal of the American Statistical Association*, 117(540):1669–1683.
- Zeldow, B., Re III, V. L., and Roy, J. (2019). A semiparametric modeling approach using bayesian additive regression trees with an application to evaluate heterogeneous treatment effects. *The annals of applied statistics*, 13(3):1989.

A An additional assumption for the theoretical results of CART

Assumption A.1. Let $f^*(\cdot) \in \mathcal{F}^h$ and $K \geq h$. For any leaf node \tilde{l}_t of the depth $K - h$ tree T_{K-h} such that $\widehat{\mathcal{R}}_{\tilde{l}_t}(\hat{f}(T_{K-h})) > \widehat{\mathcal{R}}_{\tilde{l}_t}(f^*)$, we have

$$\mathcal{IG}_h(\tilde{l}_t) \geq \frac{\left(\widehat{\mathcal{R}}_{\tilde{l}_t}(\hat{f}(T_{K-h})) - \widehat{\mathcal{R}}_{\tilde{l}_t}(f^*)\right)^2}{V^2(f^*)},$$

for some complexity constant $V(f^*)$ that depends only on $f^*(\cdot)$. Here

$$\widehat{\mathcal{R}}_{\tilde{l}_t}(\hat{f}(T_{K-h})) = \frac{1}{|\tilde{l}_t|} \sum_{i \in \tilde{l}_t} |Y_i - \hat{f}(T_{K-h})(\mathbf{Z}_i)|^2,$$

$$\widehat{\mathcal{R}}_{\tilde{l}_t}(f^*) = \frac{1}{|\tilde{l}_t|} \sum_{i \in \tilde{l}_t} |Y_i - f^*(\mathbf{Z}_i)|^2,$$

and $\mathcal{IG}_h(\tilde{l}_t)$ is the decrease in empirical risk from greedily splitting h times in the node \tilde{l}_t .

Remark A.2. Assumption A.1 is a technical condition required for the theoretical analysis of the greedy tree algorithm. It requires that any h sequential splits in the greedy tree must achieve a sufficient reduction in empirical risk. This assumption is introduced to address the technical challenges arising from the greedy structure of the tree algorithm. However, it is often difficult to verify because it depends on data-dependent quantities. Despite this stringent assumption, the greedy-based tree algorithm still exhibits a looser risk bound compared to the optimal tree.

B Proof of the Theoretical Results

In this section, we present the proofs of our theoretical findings in the main paper. We begin with introducing the notations and definitions that will be used throughout. Then we revisit

the theorems in the main paper. Finally, we provide a detailed proof of each theorem.

B.1 Notations and Definitions

We first introduce several notations that will be used for the proof, which are cited and summarized from Chapter 9.4 and Chapter 13.1 of Györfi et al. (2006).

We let Π_N be the family of all achievable partitions \mathcal{P} by growing a depth K tree on N points $\{(\mathbf{Z}_i, Y_i)\}_{i=1}^N$ and $M(\Pi_N) := \max\{|\mathcal{P}| : \mathcal{P} \in \Pi_N\}$ be the maximum number of terminal nodes among all partitions in Π_N . Given a set $\mathbf{Z}^N = \{\mathbf{Z}_1, \mathbf{Z}_2, \dots, \mathbf{Z}_N\} \subset \mathbb{R}^p$, we define $\Delta(\mathbf{Z}^N, \Pi_N)$ to be the number of different partitions $\{\mathbf{Z}^N \cap A : A \in \mathcal{P}\}$, for $\mathcal{P} \in \Pi_N$. The partitioning number $\Delta_N(\Pi_N)$ is defined by

$$\Delta_N(\Pi_N) := \max\{\Delta(\mathbf{Z}^N, \Pi_N) : \mathbf{Z}_1, \mathbf{Z}_2, \dots, \mathbf{Z}_N \in \mathbb{R}^p\}$$

which is the maximum number of different partitions of any N point set induced by elements of Π_N .

Definition B.1 (Shatter coefficient). Let \mathcal{A} be a class of subsets of \mathbb{R}^p and let $n \in \mathcal{N}$.

(a) For $z_1, \dots, z_n \in \mathbb{R}^p$ define

$$s(\mathcal{A}, \{z_1, \dots, z_n\}) = |\{A \cap \{z_1, \dots, z_n\} : A \in \mathcal{A}\}|$$

that is, $s(\mathcal{A}, \{z_1, \dots, z_n\})$ is the number of different subsets of $\{z_1, \dots, z_n\}$ of the form $A \cap \{z_1, \dots, z_n\}$, $A \in \mathcal{A}$.

(b) Let G be a subset of \mathbb{R}^p of size n . One says that \mathcal{A} shatters G if $s(\mathcal{A}, G) = 2^n$, i.e., if each subset of G can be represented in the form $A \cap G$ for some $A \in \mathcal{A}$.

(c) The n th shatter coefficient of \mathcal{A} is

$$S(\mathcal{A}, n) = \max_{\{z_1, \dots, z_n\} \subseteq \mathbb{R}^p} s(\mathcal{A}, \{z_1, \dots, z_n\})$$

That is, the shatter coefficient is the maximal number of different subsets of n points that can be picked out by sets from \mathcal{A} .

Definition B.2 (Vapnik-Chervonenkis dimension). Let \mathcal{A} be a class of subsets of \mathbb{R}^p with $\mathcal{A} \neq \emptyset$. The VC dimension (or Vapnik-Chervonenkis dimension) $V_{\mathcal{A}}$ of \mathcal{A} is defined by

$$V_{\mathcal{A}} = \sup \{n \in \mathcal{N} : S(\mathcal{A}, n) = 2^n\}$$

i.e., the VC dimension $V_{\mathcal{A}}$ is the largest integer n such that there exists a set of n points in \mathbb{R}^p which can be shattered by \mathcal{A} .

Definition B.3 (\mathcal{F}^+). We denote

$$\mathcal{F}^+ := \{\{(z, t) \in \mathbb{R}^p \times \mathbb{R}; t \leq f(z)\}; f \in \mathcal{F}\}$$

of all subgraphs of functions of \mathcal{F} .

B.2 Lemmas

Before presenting the proof, we list some useful lemmas that will be used in the proof. The first four lemmas are cited from Theorem 9.4, Theorem 9.5, Theorem 11.4, and Lemma 13.1 of Györfi et al. (2006). Lemma 5 is cited from the proof of Theorem 4.3 in Klusowski and Tian (2024).

Lemma B.4. *Let Π be a family of partitions of \mathbb{R}^p and let \mathcal{F} be a class of function $f : \mathbb{R}^p \rightarrow \mathbb{R}$. Then one has for each $z_1, \dots, z_n \in \mathbb{R}^p$ for each $\epsilon > 0$, we have*

$$\mathcal{N}_1(\epsilon, \mathcal{F} \circ \Pi, z_1^n) \leq \Delta(z_1^n, \Pi) \left\{ \sup_{x_1, \dots, x_m \in z_1^n, m \leq n} \mathcal{N}_1(\epsilon, \mathcal{F} \circ \Pi, x_1^m) \right\}^{M(\Pi)}.$$

Lemma B.5. Assume $|Y| \leq U_0$ a.s. and $U_0 \geq 1$. Let \mathcal{F} be a set of functions $f : \mathbb{R}^p \rightarrow \mathbb{R}$ and let $|f(z)| \leq U_0, U_0 \geq 1$. Then, for each $n \geq 1$,

$$\begin{aligned} & \mathbf{P} \left\{ \exists f \in \mathcal{F} : \mathbb{E}|f(Z) - Y|^2 - \mathbb{E}|f^*(Z) - Y|^2 - \frac{1}{n} \sum_{i=1}^n (|f(Z_i) - Y_i|^2 - |f^*(Z_i) - Y_i|^2) \right. \\ & \quad \left. \geq \epsilon \cdot (\alpha + \beta + \mathbb{E}|f(Z) - Y|^2 - \mathbb{E}|f^*(Z) - Y|^2) \right\} \\ & \leq 14 \sup_{Z_1^n} \mathcal{N}_1 \left(\frac{\beta\epsilon}{20U_0}, \mathcal{F}, Z_1^n \right) \exp \left(-\frac{\epsilon^2(1-\epsilon)\alpha n}{214(1+\epsilon)U_0^4} \right), \end{aligned}$$

where $\alpha, \beta > 0$ and $0 < \epsilon \leq 1/2$.

Lemma B.6. Let \mathcal{F} be an r -dimensional vector space of real functions on \mathbb{R}^p , and set

$$\mathcal{A} = \{\{\mathbf{Z} : f(\mathbf{Z}) \geq 0\} : f \in \mathcal{F}\}$$

Then

$$V_{\mathcal{A}} \leq r.$$

Lemma B.7. Let \mathcal{F} be a class of functions $f : \mathbb{R}^p \rightarrow [0, U_0]$ with $V_{\mathcal{F}^+} \geq 2$, let ν be a probability measure on \mathbb{R}^p , and let $0 < \epsilon < \frac{U_0}{4}$. Then

$$\mathcal{N}(\epsilon, \mathcal{F}, \|\cdot\|_{L_1(\nu)}) \leq \mathcal{M}(\epsilon, \mathcal{F}, \|\cdot\|_{L_1(\nu)}) \leq 3 \left(\frac{2eU_0}{\epsilon} \log \frac{3eU_0}{\epsilon} \right)^{V_{\mathcal{F}^+}}.$$

Lemma B.8.

$$\Delta_N(\Pi_N) \leq ((N-1)p)^{2^K-1} \leq (Np)^{2^K}$$

for any depth K tree partitions Π_N .

B.3 Proof of Theorem 4.2

To prove this theorem, we use a truncation technique and decompose

$$\mathbb{E}_{\mathcal{D}_n} \left(\left\| \hat{f}(T_K^{\text{OT}}) - f^* \right\|^2 \right) = \mathbb{E}_{\mathcal{D}_n} \left(\left\| \hat{f}(T_K^{\text{OT}}) - f^* \right\|^2 \cdot \mathbf{1}(E_U) \right) + \mathbb{E}_{\mathcal{D}_n} \left(\left\| \hat{f}(T_K^{\text{OT}}) - f^* \right\|^2 \cdot \mathbf{1}(E_U^c) \right).$$

where the event E_U is defined as

$$E_U := \{|Y_i| \leq U, i = 1, 2, \dots, N\}.$$

We first consider the first term $\mathbb{E}_{\mathcal{D}_n} \left(\left\| \hat{f}(T_K^{\text{OT}}) - f^* \right\|^2 \cdot \mathbf{1}(E_U) \right)$.

To bound this term, we can rewrite $\left\| \hat{f}(T_K^{\text{OT}}) - f^* \right\|^2 = E_1 + E_2$, where

$$E_1 := \left\| \hat{f}(T_K^{\text{OT}}) - f^* \right\|^2 - \frac{2}{|\mathcal{D}_n|} \left(\sum_{i \in \mathcal{D}_n} |Y_i - \hat{f}(T_K^{\text{OT}})(\mathbf{Z}_i)|^2 - \sum_{i \in \mathcal{D}_n} |Y_i - f^*(\mathbf{Z}_i)|^2 \right) - \alpha - \beta$$

and

$$E_2 := \frac{2}{|\mathcal{D}_n|} \left(\sum_{i \in \mathcal{D}_n} |Y_i - \hat{f}(T_K^{\text{OT}})(\mathbf{Z}_i)|^2 - \sum_{i \in \mathcal{D}_n} |Y_i - f^*(\mathbf{Z}_i)|^2 \right) + \alpha + \beta$$

Here α and β are positive constants that we specify later.

Since T_K^{OT} is an optimal tree and $f^* \in \mathcal{F}_h$ with the form

$$f^*(\mathbf{Z}) = \sum_{j=1}^{M(T_K^*)} \mathbf{1}_{\{\mathbf{Z} \in \mathcal{A}_j^*\}} \gamma_j^{*T} \mathbf{Z}.$$

we have

$$\frac{2}{|\mathcal{D}_n|} \left(\sum_{i \in \mathcal{D}_n} |Y_i - \hat{f}(T_K^{\text{OT}})(\mathbf{Z}_i)|^2 - \sum_{i \in \mathcal{D}_n} |Y_i - f^*(\mathbf{Z}_i)|^2 \right) \leq 0 \quad \text{and} \quad E_2 \leq \alpha + \beta.$$

Thus

$$\mathbb{E}_{\mathcal{D}_n}(E_2 \cdot \mathbf{1}(E_U)) \leq \mathbb{E}_{\mathcal{D}_n}(E_2) \leq \alpha + \beta.$$

Now it remains to bound E_1 . We let \mathcal{F}_N denote the collection of all piece-wise linear functions (bounded by U) on partitions $\mathcal{P} \in \Pi_N$.

Now, by using Lemma B.5 and choosing $\epsilon = 1/2$, we have

$$\begin{aligned} & \mathbb{P}_{\mathcal{D}_n}(E_1 \geq 0) \\ & \leq \mathbb{P}_{\mathcal{D}_n} \left(\exists f(\cdot) \in \mathcal{F}_N : \|f - f^*\|^2 \geq \frac{2}{|\mathcal{D}_n|} \left(\sum_{i \in \mathcal{D}_n} |Y_i - \hat{f}(T_K^{\text{OT}})(\mathbf{Z}_i)|^2 - \sum_{i \in \mathcal{D}_n} |Y_i - f^*(\mathbf{Z}_i)|^2 \right) + \alpha + \beta \right) \\ & \leq 14 \sup_{\mathbf{Z}^N} \mathcal{N} \left(\frac{\beta}{40U}, \mathcal{F}_N, L_1(\mathbb{P}_{\mathbf{Z}^N}) \right) \exp \left(-\frac{\alpha N}{2568U^4} \right), \end{aligned}$$

where $\mathbf{Z}^N = \{\mathbf{Z}_1, \mathbf{Z}_2, \dots, \mathbf{Z}_N\} \subset \mathbb{R}^p$ and $\mathcal{N}(r, \mathcal{F}_N, L_1(\mathbb{P}_{\mathbf{Z}^N}))$ is the covering number for \mathcal{F}_N by balls of radius $r > 0$ in $L_1(\mathbb{P}_{\mathbf{Z}^N})$ with respect to the empirical discrete measure $\mathbb{P}_{\mathbf{Z}^N}$ on \mathbf{Z}^N .

By Lemma B.6, we have the following result: If \mathcal{F} is a class of linear functions on \mathbb{R}^p , we have

$$V_{\mathcal{F}^+} \leq p + 1.$$

We note that the collection of all piece-wise linear functions \mathcal{F}_N can be written as $\mathcal{F} \circ \Pi_N$ as in Lemma B.4. Thus by Lemma B.4, we can show

$$\mathcal{N} \left(\frac{\beta}{40U}, \mathcal{F}_N, L_1(\mathbb{P}_{\mathbf{Z}^N}) \right) \leq \Delta_N(\Pi_N) \left\{ \sup_{\mathbf{x}_1, \dots, \mathbf{x}_m \in \mathbf{Z}_1^n, m \leq n} \mathcal{N} \left(\frac{\beta}{40U}, \mathcal{F}, L_1(\mathbb{P}_{\mathbf{x}_{1:m}}) \right) \right\}^{M(\Pi)}$$

We now can use Lemma B.7 to bound the following empirical covering number by

$$\begin{aligned} \sup_{\mathbf{x}_1, \dots, \mathbf{x}_m \in \mathbf{Z}_1^n, m \leq n} \mathcal{N}\left(\frac{\beta}{40U}, \mathcal{F}, L_1(\mathbb{P}_{\mathbf{x}_{1:m}})\right) &\leq 3 \left(\frac{160eU^2}{\beta} \log \frac{240eU^2}{\beta}\right)^{V_{\mathcal{F}+}} \\ &\leq 3 \left(\frac{240eU^2}{\beta}\right)^{2V_{\mathcal{F}+}} \\ &\leq 3 \left(\frac{240eU^2}{\beta}\right)^{2(p+1)}. \end{aligned}$$

Then we can get

$$\mathcal{N}\left(\frac{\beta}{40U}, \mathcal{F}_N, L_1(\mathbb{P}_{\mathbf{Z}^N})\right) \leq \Delta_N(\Pi_N) \left(3 \left(\frac{240eU^2}{\beta}\right)^{p+1}\right)^{2M(\Pi_N)} \leq \Delta_N(\Pi_N) \left(\frac{C_0^{p+1}U^{2p+2}}{\beta^{p+1}}\right)^{2K+1}.$$

Here C_0 is a large enough constant.

By Lemma B.8 we have

$$\Delta_N(\Pi_N) \leq (Np)^{2K}.$$

We therefore can bound the covering number by

$$\mathcal{N}\left(\frac{\beta}{40U}, \mathcal{F}_N, L_1(\mathbb{P}_{\mathbf{Z}^N})\right) \leq (Np)^{2K} \left(\frac{C_0^{p+1}U^{2p+2}}{\beta^{p+1}}\right)^{2K+1}.$$

Since $\hat{f}(T_K^{\text{OT}})(\cdot) \in \mathcal{F}_N$, we have

$$\mathbb{P}_{\mathcal{D}_n}(E_1 \geq 0 | E_U) \leq 14(Np)^{2K} \left(\frac{C_0^{p+1}U^{2p+2}}{\beta^{p+1}}\right)^{2K+1} \exp\left(-\frac{\alpha N}{2568U^4}\right).$$

If we choose

$$\alpha = C'_1 \cdot \frac{U^4 2^K \log(N^{p+1}p)}{N} \text{ and } \beta = C'_2 \cdot \frac{U^2}{N}$$

with positive constants C'_1 and C'_2 , then we have

$$\begin{aligned}
& 14(Np)^{2K} \left(\frac{C_0^{p+1} U^{2p+2}}{\beta^{p+1}} \right)^{2^{K+1}} \exp \left(-\frac{\alpha N}{2568U^4} \right) \\
& \leq 14(Np)^{2K} \left(\frac{C_0^{p+1} N^{p+1} U^{2p+2}}{C_2'^{p+1} \cdot U^{2p+2}} \right)^{2^{K+1}} \exp \left(-\frac{C'_1 \cdot U^4 2^K \log(N^{p+1}p)}{2568U^4} \right) \\
& \leq 14(Np)^{2K} \left(\frac{C_0^{p+1} N^{p+1}}{C_2'^{p+1}} \right)^{2^{K+1}} \exp \left(-\frac{C'_1 \cdot 2^K \log(N^{p+1}p)}{2568} \right) \\
& \leq 14N^{2K} N^{(p+1) \cdot 2^{K+1}} N^{-(p+1) \frac{C'_1 \cdot 2^K}{2568}} p^{2K} \left(\frac{C_0^{p+1}}{C_2'^{p+1}} \right)^{2^{K+1}} p^{-\frac{C'_1 \cdot 2^K}{2568}} \\
& = 14N^{(2p+3) \cdot 2^K} N^{-(p+1) \frac{C'_1 \cdot 2^K}{2568}} p^{2K} \left(\frac{C_0^{p+1}}{C_2'^{p+1}} \right)^{2^{K+1}} p^{-\frac{C'_1 \cdot 2^K}{2568}}.
\end{aligned}$$

If we further let C'_1 be large enough so that $C'_1/2568 \geq 3$ and $C'_2 \geq C_0$, then we are able to show

$$14N^{(2p+3) \cdot 2^K} N^{-(p+1) \frac{C'_1 \cdot 2^K}{2568}} p^{2K} \left(\frac{C_0^{p+1}}{C_2'^{p+1}} \right)^{2^{K+1}} p^{-\frac{C'_1 \cdot 2^K}{2568}} \leq C' N^{-2K} \leq C'/N.$$

for some universal constant C' . Therefore, $\mathbb{P}_{\mathcal{D}_n}(E_1 \geq 0 | E_U) \leq C'/N$.

Furthermore, we have $E_1 \leq \left\| \hat{f}(T_K^{\text{OT}}) - f^* \right\|^2 + 2 \|Y - f^*\|_{\mathcal{D}_n}^2$. Condition on the event E_U ,

$$E_1 \leq \left\| \hat{f}(T_K^{\text{OT}}) - f^* \right\|^2 + 2 \|Y - f^*\|_{\mathcal{D}_n}^2 \leq 12U^2.$$

Thus,

$$\mathbb{E}_{\mathcal{D}_n}(E_1 \cdot \mathbf{1}(E_U)) \leq 12U^2 \mathbb{P}_{\mathcal{D}_n}(E_1 \geq 0 | E_U) \leq 12C'U^2/N.$$

With the choices of α and β , we then have

$$\begin{aligned}
\mathbb{E}_{\mathcal{D}_n} \left(\left\| \hat{f}(T_K^{\text{OT}}) - f^* \right\|^2 \cdot \mathbf{1}(E_U) \right) &= \mathbb{E}_{\mathcal{D}_n}(E_1 \cdot \mathbf{1}(E_U)) + \mathbb{E}_{\mathcal{D}_n}(E_2 \cdot \mathbf{1}(E_U)) \\
&\leq C'' \left(\frac{U^4 2^K \log(N^{p+1}p)}{N} + \frac{U^2}{N} \right)
\end{aligned} \tag{3}$$

where C'' is a positive universal constant.

Next, we consider the second term $\mathbb{E}_{\mathcal{D}_n} \left(\left\| \hat{f}(T_K^{\text{OT}}) - f^* \right\|^2 \cdot \mathbf{1}(E_U^c) \right)$. If we choose U such that $U \geq \|f^*\|_\infty$, we will have

$$\mathbb{P}_{\mathcal{D}_n}(E_U^c) = \mathbb{P}(\cup_{i=1}^N |Y_i| > U) \leq N\mathbb{P}(|y_1| > U) \leq N\mathbb{P}(|\varepsilon| > U - \|f^*\|_\infty) \leq 2N \exp\left(-\frac{(U - \|f^*\|_\infty)^2}{2\sigma^2}\right).$$

Since we have

$$\left\| \hat{f}(T_K^{\text{OT}}) \right\|_\infty = \sup_{\mathbf{Z} \in \mathcal{Z}} \left| \sum_{\tilde{l}_t \in \mathcal{T}_L(T_K^{\text{OT}})} \mathbf{1}_{(\mathbf{Z} \in \tilde{l}_t)} (\hat{\gamma}_{\tilde{l}_t})^T \mathbf{Z} \right| \leq \sup_{\tilde{l}_t \in \mathcal{T}_L(T_K^{\text{OT}})} \|\hat{\gamma}_{\tilde{l}_t}\|_1 \leq B,$$

and

$$\|f^*\|_\infty = \sup_{\mathbf{Z} \in \mathcal{Z}} \left| \sum_{\tilde{l}_t \in \mathcal{T}_L(T_K^*)} \mathbf{1}_{\{\mathbf{Z} \in \tilde{l}_t\}} \gamma_{\tilde{l}_t}^{*T} \mathbf{Z} \right| \leq \sup_{\tilde{l}_t \in \mathcal{T}_L(T_K^*)} \|\gamma_{\tilde{l}_t}^*\|_1 \leq B,$$

We now have

$$\mathbb{E}_{\mathcal{D}_n} \left(\left\| \hat{f}(T_K^{\text{OT}}) - f^* \right\|^2 \mathbf{1}(E_U^c) \right) \leq 4B^2 \mathbb{P}_{\mathcal{D}_n}(E_U^c) \leq 8B^2 N \exp\left(-\frac{(U - \|f^*\|_\infty)^2}{2\sigma^2}\right).$$

Choosing $U = B + \sqrt{2\sigma} \sqrt{2 \log(N)}$ yields

$$8B^2 N \exp\left(-\frac{(U - \|f^*\|_\infty)^2}{2\sigma^2}\right) \leq 8B^2 N \exp\left(-\frac{(U - B)^2}{2\sigma^2}\right) = 8B^2 N \exp(-2 \log(N)) = \frac{8B^2}{N}.$$

and therefore we have

$$\mathbb{E}_{\mathcal{D}_n} \left(\left\| \hat{f}(T_K^{\text{OT}}) - f^* \right\|^2 \mathbf{1}(E_U^c) \right) \leq \frac{8B^2}{N}.$$

With this choice of U , we can combine the bound in Equation (3) and obtain

$$\begin{aligned} \mathbb{E}_{\mathcal{D}_n} \left(\left\| \hat{f}(T_K^{\text{OT}}) - f^* \right\|^2 \right) &\leq C'' \left(\frac{U^4 2^K \log(N^{p+1}p)}{N} + \frac{U^2}{N} \right) + \frac{8B^2}{N} \\ &\leq C_1 \frac{2^K \log^2(N) ((p+1) \cdot \log(N) + \log(p))}{N}. \end{aligned}$$

for some constant $C_1 > 0$ that depends only on B and σ^2 .

B.4 Proof of Theorem 4.3

The proof of Theorem 4.3 is similar to the proof of Theorem 4.2. The main difference is the bound on E_2 .

$$E_2 := \frac{2}{|\mathcal{D}_n|} \left(\sum_{i \in \mathcal{D}_n} |Y_i - \hat{f}(T_K^{\text{CART}})(\mathbf{Z}_i)|^2 - \sum_{i \in \mathcal{D}_n} |Y_i - f^*(\mathbf{Z}_i)|^2 \right) + \alpha + \beta$$

with T_K^{OT} replaced by T_K^{CART} . We know that T_K^{CART} is a sub-optimal tree, so

$$\frac{2}{|\mathcal{D}_n|} \left(\sum_{i \in \mathcal{D}_n} |Y_i - \hat{f}(T_K^{\text{CART}})(\mathbf{Z}_i)|^2 - \sum_{i \in \mathcal{D}_n} |Y_i - f^*(\mathbf{Z}_i)|^2 \right) \leq 0$$

no longer holds. To bound this term, we need to introduce an additional assumption, which is Assumption 2.

With Assumption A.1, following Lemma D.1 in Klusowski and Tian (2024) we have

$$\frac{1}{|\mathcal{D}_n|} \left(\sum_{i \in \mathcal{D}_n} |Y_i - \hat{f}(T_K^{\text{CART}})(\mathbf{Z}_i)|^2 - \sum_{i \in \mathcal{D}_n} |Y_i - f^*(\mathbf{Z}_i)|^2 \right) \leq \frac{V(f^*)h}{K + 2h + 1}.$$

Thus

$$\mathbb{E}_{\mathcal{D}_n} (E_2 \cdot \mathbf{1}(E_U)) \leq \mathbb{E}_{\mathcal{D}_n} (E_2) \leq \frac{2V(f^*)h}{K + 2h + 1} + \alpha + \beta.$$

By using similar proof in Theorem 4.2 with T_K^{OT} replaced by T_K^{CART} , we have

$$\begin{aligned}
\mathbb{E}_{\mathcal{D}_n} \left(\left\| \hat{f} (T_K^{\text{CART}}) - f^* \right\|^2 \right) &\leq \frac{2V(f^*)h}{K+2h+1} + C'' \left(\frac{U^4 2^K \log(N^{p+1}p)}{N} + \frac{U^2}{N} \right) + \frac{8B^2}{N} \\
&\leq C_1 \frac{2^K \log^2(N) ((p+1) \cdot \log(N) + \log(p))}{N} + \frac{2V(f^*)h}{K+2h+1}.
\end{aligned}$$

Let $C_0 = 2V(f^*)$ then we finish the proof of Theorem 4.3.

C Additional figures and tables in the case study

	Black N=237 (%)
Sex	
Female	145 (61.2)
Male	92 (38.8)
APOE2	
0	195 (82.3)
1	40 (16.9)
2	2 (0.8)
APOE4	
0	154 (65.0)
1	73 (30.8)
2	10 (4.2)
Education (years)	
Min	7
Median	14
Max	20
Age	
50-55	34 (14.3)
55-60	55 (23.2)
60-65	59 (24.9)
65-70	47 (19.8)
70-75	32 (13.5)
75-80	5 (2.1)
80-85	3 (1.3)
85-90	2 (0.8)
Amyloid-beta (Treatment)	
$A\beta < 10$	171 (72.2)
$A\beta \geq 10$	66 (27.8)
Tau in Medial Temporal Lobe (Tau_1)	
Min	0.675
Median	1.276
Max	2.215
Tau in the neocortex (Tau_2)	
Min	0.627
Median	1.066
Max	1.956

Table 1: Demographic characteristics of black participants in HABS-HD dataset

Variable	Estimate	P-Value
Intercept	-0.031	0.813
Treatment	0.132	0.548
Sex (group 4)	0.195	0.445
Sex (group 1/2/3)	-0.178	0.239
APOE2	-0.136	0.397
APOE4	0.094	0.524
Edu (group 3)	1.298	0.000
Edu (group 1/2/4)	0.515	0.000
Age	-0.241	0.006
Tau_1	0.025	0.842
Tau_2 (group 1/3)	0.590	0.011
Tau_2 (group 2/4)	-0.328	0.108
Treatment \times Sex (group 2)	-0.214	0.582
Treatment \times Sex (group 1/3/4)	0.360	0.287
Treatment \times APOE2	-0.256	0.444
Treatment \times APOE4	0.238	0.386
Treatment \times Edu	-0.177	0.356
Treatment \times Age	-0.018	0.903
Treatment \times Tau_1 (group 1/2)	0.187	0.522
Treatment \times Tau_1 (group 3/4)	-0.292	0.191
Treatment \times Tau_2 (group 1/2/4)	0.418	0.158
Treatment \times Tau_2 (group 3)	-0.962	0.000

Table 2: Coefficients Estimates and p-values for FOCT (Rounded to 3 Decimal Places)

Variable	Estimate	P-value
Intercept	0.368	0.555
Treatment	0.576	0.809
Sex	-0.367	0.219
APOE2	-0.563	0.067
APOE4	0.462	0.162
Edu	0.525	0.018
Age	0.163	0.340
Tau_1	0.095	0.701
Tau_2	0.126	0.865
Treatment \times Sex	-1.002	0.512
Treatment \times APOE2	-1.443	0.310
Treatment \times APOE4	1.526	0.129
Treatment \times Edu	-0.401	0.518
Treatment \times Age	0.999	0.254
Treatment \times Tau_1	0.414	0.679
Treatment \times Tau_2	0.333	0.725

Table 3: Coefficient estimates and p-values of subgroup 1 for CT-CART/OCT (Rounded to 3 Decimal Places)

Variable	Estimate	P-value
Intercept	0.715	0.098
Treatment	-1.111	0.161
Sex	-0.777	0.026
APOE2	0.628	0.146
APOE4	0.113	0.712
Edu	2.211	0.001
Age	-0.707	0.000
Tau_1	0.323	0.274
Tau_2	-0.307	0.528
Treatment \times Sex	1.345	0.011
Treatment \times APOE2	-2.459	0.000
Treatment \times APOE4	1.347	0.020
Treatment \times Edu	-1.783	0.218
Treatment \times Age	0.291	0.248
Treatment \times Tau_1	-0.738	0.066
Treatment \times Tau_2	-0.369	0.486

Table 4: Coefficient estimates and p-values of subgroup 2 for CT-CART/OCT (Rounded to 3 Decimal Places)

Variable	Estimate	P-value
Intercept	0.016	0.916
Treatment	0.467	0.158
Sex	0.247	0.151
APOE2	0.171	0.391
APOE4	-0.005	0.975
Edu	0.393	0.010
Age	-0.072	0.448
Tau_1	0.071	0.693
Tau_2	-0.220	0.294
Treatment \times Sex	-0.889	0.013
Treatment \times APOE2	-0.158	0.719
Treatment \times APOE4	-0.735	0.037
Treatment \times Edu	-0.141	0.639
Treatment \times Age	0.063	0.753
Treatment \times Tau_1	0.081	0.777
Treatment \times Tau_2	-0.348	0.193

Table 5: Coefficient estimates and p-values of subgroup 3 for CT-CART/OCT (Rounded to 3 Decimal Places)

D Additional simulation details

D.1 Parameters specification

In our main simulation setup, we set the parameters as

- (1) $\delta_1 = \delta_2 = \delta_3 = \delta_4 = 0$.
- (2) $\mu_1 = \mu_3 = 1, \mu_2 = \mu_4 = 2$.
- (3) $\alpha_1 = [1, 1, 2]^\top, \alpha_2 = [1, 1, 4]^\top, \alpha_3 = [1, 1, 3]^\top, \alpha_4 = [1, 1, 5]^\top$.
- (4) $\beta_1 = \beta_2 = [0, 1, 0]^\top, \beta_3 = \beta_4 = [1, 1, 2]^\top$.

D.2 Explicit forms of SATE

The SATE for any given \mathbf{X}_i is $\tau(\mathbf{X}_i, \Pi^*, \rho) = \sum_{m=1}^4 \mathbf{1}_{(\mathbf{X}_i \in \mathcal{A}_m^*)} \cdot \tilde{\mu}_m(\rho)$. Here $\tilde{\mu}_1(\rho), \dots, \tilde{\mu}_4(\rho)$ are closed-form functions depending on ρ .

- $\tilde{\mu}_1(\rho) = 1 + \mathbb{E}[X_2 | X_1 < 0, X_2 < 0]$,
- $\tilde{\mu}_2(\rho) = 2 + \mathbb{E}[X_2 | X_1 < 0, X_2 \geq 0]$,
- $\tilde{\mu}_3(\rho) = 1 + \mathbb{E}[X_1 + X_2 + 2X_3 | X_1 \geq 0, X_2 < 0]$,
- $\tilde{\mu}_4(\rho) = 2 + \mathbb{E}[X_1 + X_2 + 2X_3 | X_1 \geq 0, X_2 \geq 0]$.

Here $X_1 \sim \mathcal{N}(0, 1)$ and $(X_2, X_3)^T \sim \mathcal{N}(\mathbf{0}, \Sigma)$ and Σ is a 2×2 matrix with 1s on the diagonal and ρ in the off-diagonal entries. We have

- $\tilde{\mu}_1(\rho) = 1 + \mathbb{E}[X_2 | X_1 < 0, X_2 < 0] = 1 - \sqrt{\frac{2}{\pi}}$,
- $\tilde{\mu}_2(\rho) = 2 + \mathbb{E}[X_2 | X_1 < 0, X_2 \geq 0] = 2 + \sqrt{\frac{2}{\pi}}$,
- $\tilde{\mu}_3(\rho) = 1 + \mathbb{E}[X_1 + X_2 + 2X_3 | X_1 \geq 0, X_2 < 0] = 1 - 2\rho\sqrt{\frac{2}{\pi}}$,
- $\tilde{\mu}_4(\rho) = 2 + \mathbb{E}[X_1 + X_2 + 2X_3 | X_1 \geq 0, X_2 \geq 0] = 2 + (2\rho + 2)\sqrt{\frac{2}{\pi}}$.

Calculation: Given X_2 is a standard normal random variable, the conditional expectation $\mathbb{E}[X_2|X_1 < 0, X_2 < 0] = \mathbb{E}[X_2|X_2 < 0]$ can be computed by using properties of the normal distribution. The expected value of a truncated normal distribution for a standard normal variable conditioned on $X_2 < 0$ is given by:

$$\mathbb{E}[X_2|X_2 < 0] = \frac{-\frac{1}{\sqrt{2\pi}}}{\frac{1}{2}} = -\sqrt{\frac{2}{\pi}}.$$

Similarly

$$\mathbb{E}[X_2|X_2 \geq 0] = \frac{-\frac{1}{\sqrt{2\pi}}}{\frac{1}{2}} = \sqrt{\frac{2}{\pi}}.$$

Then we have

- $\tilde{\mu}_1(\rho) = 1 + \mathbb{E}[X_2|X_1 < 0, X_2 < 0] = 1 - \sqrt{\frac{2}{\pi}},$
- $\tilde{\mu}_2(\rho) = 2 + \mathbb{E}[X_2|X_1 < 0, X_2 \geq 0] = 2 + \sqrt{\frac{2}{\pi}}.$
- $\tilde{\mu}_3(\rho) = 1 + \mathbb{E}[X_1 + X_2 + 2X_3|X_1 \geq 0, X_2 < 0],$
- $\tilde{\mu}_4(\rho) = 2 + \mathbb{E}[X_1 + X_2 + 2X_3|X_1 \geq 0, X_2 \geq 0].$

we first calculate

$$\mathbb{E}[X_1 + X_2 + 2X_3|X_1 \geq 0, X_2 < 0] = \mathbb{E}[X_2 + 2X_3|X_2 < 0] + \mathbb{E}[X_1|X_1 \geq 0].$$

To calculate the conditional expectation:

$$\mathbb{E}[X_2 + 2X_3 | X_2 < 0],$$

Where X_2 and X_3 are jointly standard normal random variables with correlation coefficient ρ , we decompose the expectation into the sum of individual expectations:

$$\mathbb{E}[X_2 + 2X_3 | X_2 < 0] = \mathbb{E}[X_2 | X_2 < 0] + 2\mathbb{E}[X_3 | X_2 < 0].$$

Since X_2 and X_3 are jointly normal, the conditional distribution of X_3 given X_2 is normal with $\mathbb{E}[X_3 | X_2] = \rho X_2$. To find $\mathbb{E}[X_3 | X_2 < 0]$, we take the expectation over all $X_2 < 0$:

$$\mathbb{E}[X_3 | X_2 < 0] = \mathbb{E}_{X_2} [\mathbb{E}[X_3 | X_2] | X_2 < 0] = \mathbb{E}_{X_2} [\rho X_2 | X_2 < 0] = \rho \mathbb{E}[X_2 | X_2 < 0].$$

Now, we substitute the computed expectations back into the original expression:

$$\begin{aligned} \mathbb{E}[X_2 + 2X_3 | X_2 < 0] &= \mathbb{E}[X_2 | X_2 < 0] + 2\mathbb{E}[X_3 | X_2 < 0] \\ &= (1 + 2\rho) \cdot \mathbb{E}[X_2 | X_2 < 0] \\ &= -\sqrt{\frac{2}{\pi}}(1 + 2\rho). \end{aligned}$$

With $\mathbb{E}[X_1 | X_1 \geq 0] = \sqrt{\frac{2}{\pi}}$ we have

$$\mathbb{E}[X_1 + X_2 + 2X_3 | X_1 \geq 0, X_2 < 0] = -2\rho\sqrt{\frac{2}{\pi}}.$$

Similarly,

$$\mathbb{E}[X_1 + X_2 + 2X_3 | X_1 \geq 0, X_2 \geq 0] = (2\rho + 2)\sqrt{\frac{2}{\pi}}.$$

Thus we can show

- $\tilde{\mu}_3(\rho) = 1 + \mathbb{E}[X_1 + X_2 + 2X_3 | X_1 \geq 0, X_2 < 0] = 1 - 2\rho\sqrt{\frac{2}{\pi}},$
- $\tilde{\mu}_4(\rho) = 2 + \mathbb{E}[X_1 + X_2 + 2X_3 | X_1 \geq 0, X_2 \geq 0] = 2 + (2\rho + 2)\sqrt{\frac{2}{\pi}}.$

E Additional Experiments

E.1 Smaller sample size $n = 100$ (OCT can perform poorly in extremely small samples).

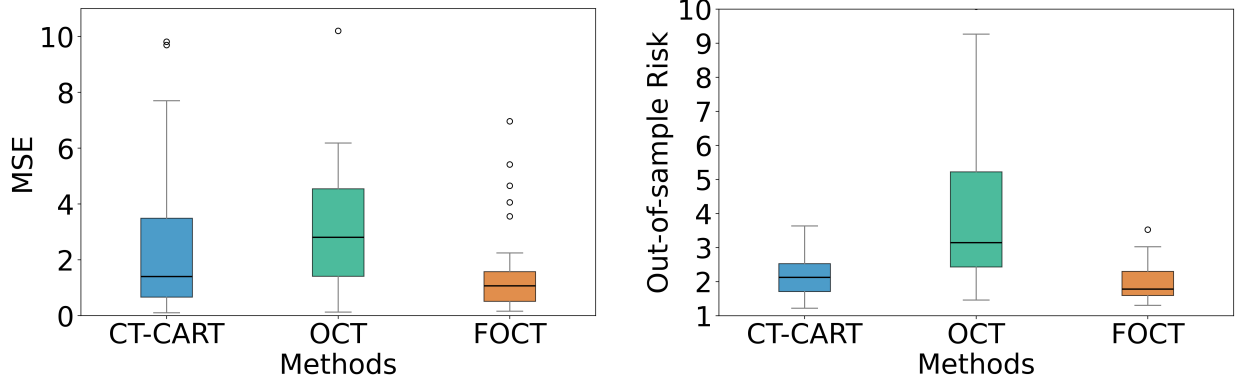
We also conduct a series of simulations with smaller sample sizes, where overfitting issues become more pronounced. Under these conditions, the advantages of adopting FOCT are further underscored. We tune the λ in the grid $\Lambda = \{1/500 * i | i = 1, \dots, 5\}$ in this section.

E.1.1 The dimension of variables $d = 3$, imbalanced treatment and control groups with $p = 0.3$, and $\rho = 0.5$

We reduce the sample size to $n = 100$, thereby exacerbating the overfitting issue. Across 50 Monte Carlo simulations, CT-CART identifies the correct tree structure only 10 times, OCT 20 times, and FOCT 39 times—indicating a clear advantage for FOCT. In terms of SATE estimation precision and out-of-sample risk, OCT performs the worst, while FOCT performs the best (Figure 5a and Figure 5b). This disparity arises because, with such a small sample size, overfitting is extreme: OCT, which optimizes the tree structure solely based on training data, suffers most from overfitting, resulting in poor generalization. In contrast, the fusion constraint in FOCT mitigates overfitting and improves out-of-sample performance. Although CT-CART is less prone to overfitting in this scenario, it struggles to accurately identify subgroups. Overall, FOCT outperforms the other methods in this scenario, achieving higher subgroup identification accuracy, better SATE estimation, and lower out-of-sample risk.

E.1.2 The dimension of variables $d = 5$, imbalanced treatment and control groups with $p = 0.3$, and $\rho = 0.5$

We also explore a setting where we introduce additional irrelevant predictors to increase the complexity of subgroup identification and SATE estimation. Specifically, we add two

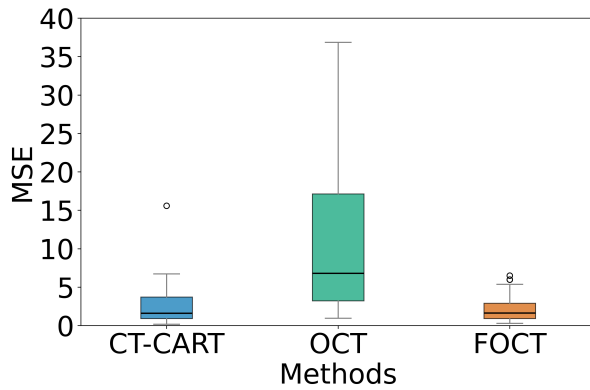


(a) $n = 100$, $p = 0.3$, $\rho = 0.5$ and $d = 3$

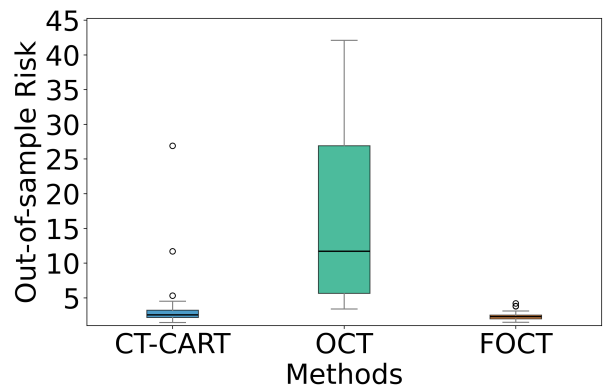
(b) $n = 100$, $p = 0.3$, $\rho = 0.5$ and $d = 3$

Figure 5: Boxplot of mean square error (MSE) of SATE estimation and out-of-sample risk for different methods with $n = 100$, $p = 0.3$, $\rho = 0.5$ and $d = 3$ across 50 Monte Carlo simulations.

independent, standard normal variables X_4 and X_5 into the leaf-level regression model, extending it to $Y \sim [T, X_1, X_2, X_3, X_4, X_5, TX_1, TX_2, TX_3, TX_4, TX_5]$ while keeping the data-generating process unchanged. Including irrelevant covariates intensifies the overfitting problem, as demonstrated by results from 50 Monte Carlo simulations: CT-CART detects the correct tree structure only 9 times, OCT 6 times, and FOCT 22 times. A similar trend emerges for SATE estimation precision and out-of-sample risk, mirroring the findings in Section E.1.1 (Figure 6a and Figure 6b). OCT, which relies purely on training data to find the optimal tree structure, suffers most from overfitting and thus exhibits poor out-of-sample performance. In contrast, FOCT’s fusion constraint mitigates overfitting, yielding superior performance on both SATE estimation and out-of-sample risk. Notably, FOCT also demonstrates a slight edge over CT-CART in these measures (Figure 7a and Figure 7b).

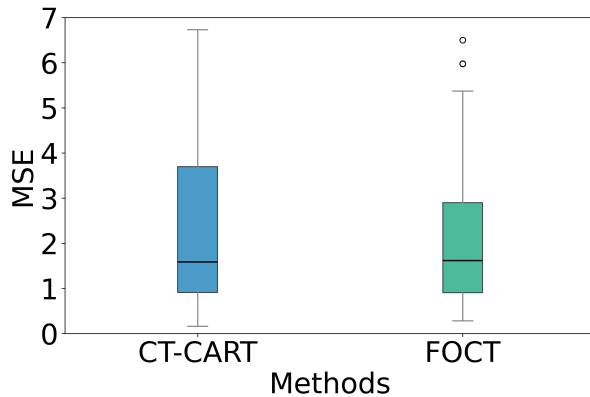


(a) $n = 100$, $p = 0.3$, $\rho = 0.5$ and $d = 5$

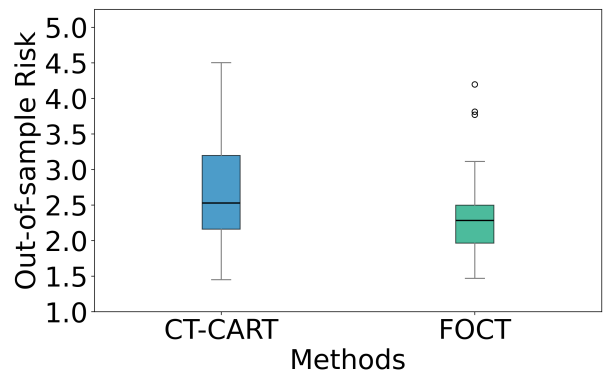


(b) $n = 100$, $p = 0.3$, $\rho = 0.5$ and $d = 5$

Figure 6: Boxplot of mean square error (MSE) of SATE estimation and out-of-sample risk for different methods with $n = 100$, $p = 0.3$, $\rho = 0.5$ and $d = 5$ across 50 Monte Carlo simulations.



(a) $n = 100$, $p = 0.3$, $\rho = 0.5$ and $d = 5$



(b) $n = 100$, $p = 0.3$, $\rho = 0.5$ and $d = 5$

Figure 7: Boxplot of mean square error (MSE) of SATE estimation and out-of-sample risk for CT-CART and FOCT with $n = 100$, $p = 0.3$, $\rho = 0.5$ and $d = 5$ across 50 Monte Carlo simulations.

E.2 Balanced treatment and control groups with $p = 0.5$ and smaller correlation between X_2 and X_3 : $\rho = 0.5$

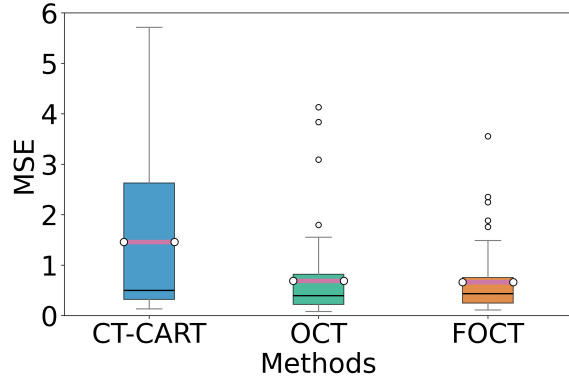
In this scenario, we set $p = 0.5$ in the equation $T \sim \text{Bernoulli}(p)$ to generate balanced treatment and control groups. We also set the parameter ρ to 0.5, thereby reducing the correlation between X_2 and X_3 . This setup mimics conditions with lower overfitting levels and decreased correlation between an actual split variable (X_2) and a spurious split variable (X_3). Consequently, we expect all three methods to exhibit improved performance. To compare their performances, we evaluate subgroup identification accuracy, SATE estimation precision, and out-of-sample risk across 50 Monte Carlo simulations. We tune the λ in the grid $\Lambda = \{1/10000 * i | i = 1, \dots, 20\}$

In this scenario, CT-CART identifies the correct tree structure 37 times, whereas OCT does so 46 times and FOCT 48 times. The superior performance of OCT and FOCT stems from their ability to yield optimal tree structures. Regarding SATE estimation precision and out-of-sample risk, OCT/FOCT again outperforms CT-CART, as reflected by smaller and more stable mean squared errors (MSEs) and out-of-sample risks (Figures 8a and 8b). However, the performance gap between OCT and FOCT narrows in this setting, because the overfitting issue is less pronounced.

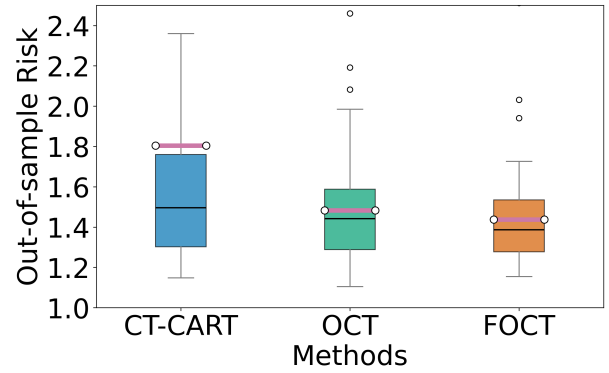
E.3 Smaller correlation $\rho = 0.6$ between X_2 and X_3

We let $\rho = 0.6$ and fix other parameters in the setup of the main paper. Then we compare the performances of different methods in terms of SATE estimation precision and out-of-sample risk.

With a smaller ρ , these three methods become more powerful in detecting the correct tree structures: FOCT (87 times), OCT (82 times), and CT-CART (65 times). In terms of SATE estimation precision and out-of-sample risk, FOCT still performs better than the other two methods, with smaller and more stable MSE and out-of-sample risk, as shown in Figure 9a



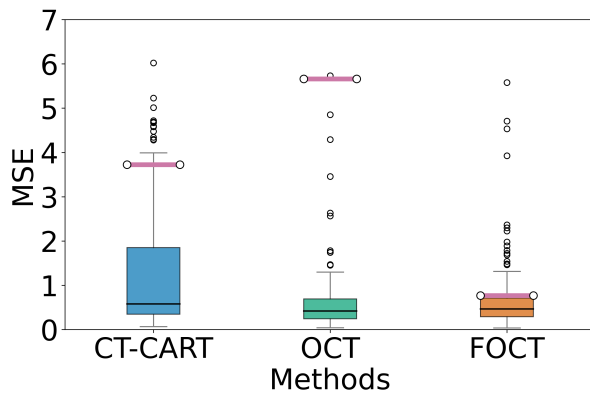
(a) $n = 200$, $\rho = 0.5$, $p = 0.5$ and $d = 3$



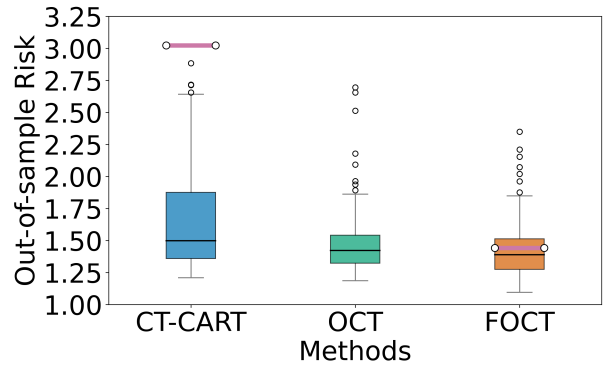
(b) $n = 200$, $\rho = 0.5$, $p = 0.5$ and $d = 3$

Figure 8: Boxplot of mean square error (MSE) of SATE estimation and out-of-sample risk for different methods with $\rho = 0.5$, $p = 0.5$, $n = 200$, and $d = 3$ across 50 Monte Carlo simulations. The purple line is the mean of MSE (or out-of-sample risk) across 50 Monte Carlo simulations for each method.

and Figure 9b.



(a) $n = 200$, $\rho = 0.6$, $p = 0.3$ and $d = 3$



(b) $n = 200$, $\rho = 0.6$, $p = 0.3$ and $d = 3$

Figure 9: Boxplot of mean square error (MSE) of SATE estimation and out-of-sample risk for different methods with $\rho = 0.6$ across 100 Monte Carlo simulations. The purple line is the mean of MSE (or out-of-sample risk) across 100 Monte Carlo simulations for each method. The purple line for OCT in Figure 9b is above 3.25 and not shown.

F Mixed integer optimization framework

MIO refers to the optimization problem involving both integer variables (which can take on only whole number values) and continuous variables (which can take on any real number values). The feasibility of this MIO-based optimal partition searching approach is bolstered by significant algorithmic advancements in integer optimization and hardware enhancements over the past 25 years. The general mixed integer optimization problem takes the form

$$\begin{aligned} & \min_{\boldsymbol{\alpha} \in \mathbb{R}^m} \boldsymbol{\alpha}^T \mathbf{Q} \boldsymbol{\alpha} + \boldsymbol{\alpha}^T \mathbf{u} \\ \text{s.t. } & \mathbf{A} \boldsymbol{\alpha} \leq \mathbf{v}, \\ & \alpha_j \in \{0, 1\}, \quad j \in \mathcal{I}, \\ & \alpha_j \geq 0, \quad j \notin \mathcal{I}. \end{aligned}$$

where $\mathbf{u} \in \mathbb{R}^m$, $\mathbf{A} \in \mathbb{R}^{h \times m}$, $\mathbf{v} \in \mathbb{R}^h$, and $\mathbf{Q} \in \mathbb{R}^{m \times m}$ is positive semi-definite. $\boldsymbol{\alpha}$ is the mixture of discrete and continuous components and \mathcal{I} is used to identify the binary components of $\boldsymbol{\alpha}$. Any optimization problem that can be expressed in this form qualifies as a mixed integer optimization problem and can be solved using popular MIO solvers such as Gurobi (Gurobi Optimization, LLC, 2024).

G Detailed notations in Algorithm 1

- We use $[n]$ to represent the integer from 1 to n .
- To mathematically represent the tree structure, we divide its nodes into two classes: \mathcal{T}_B , the set of branch nodes where splits occur, and \mathcal{T}_L , the collection of leaf nodes, each corresponding to a final identified subgroup.
- We denote the parent node of branch node t' as $\mathbf{p}(t')$ and the collection of its ancestors in the left (right) branch as $\mathcal{L}(t')$ ($\mathcal{R}(t')$).

- To allow for partially grown trees (where the number of leaf nodes is less than 2^D when the tree depth is D), we introduce binary variables $\{l_{t'}\}_{t' \in \mathcal{T}_L}$, with $l_{t'} = 0$ indicating that leaf node t' is empty.
- We also introduce a binary vector $\mathbf{a}_{t'} \in \{0, 1\}^d$ and a variable $b_{t'}$ to model the split of branch nodes $t' \in \mathcal{T}_B$. Here $\mathbf{a}_{t'}$ determine the split variable in $t' \in \mathcal{T}_B$ and $b_{t'}$ is the cutoff of this split variable. For example, $a_{t'j} = 1$ indicates that in branch node t' , the sample is divided into two partitions: $\{(\mathbf{X}_i, T_i, Y_i) \mid \mathbf{X}_i \in t', X_{ij} < b_{t'}\}$ and $\{(\mathbf{X}_i, T_i, Y_i) \mid \mathbf{X}_i \in t', X_{ij} \geq b_{t'}\}$.
- To accommodate branch nodes with no split, we use binary variables $d_{t'}$ with $d_{t'} = 0$ indicating no split occurs in branch node $t' \in \mathcal{T}_B$.
- To allow for the parameter fusion, we further introduce binary variables $\{r_{jt_1t_2}\}_{j=1}^{2d+2}$ to indicate whether we fuse two parameters on the same covariates in different subpopulations, with value $r_{jt_1t_2} = 1$ indicating that $\gamma_{t_1j} = \gamma_{t_2j}$ and value $r_{jt_1t_2} = 0$ indicating no fusion constraints between γ_{t_1j} and γ_{t_2j} .

H Causal identification

We use the potential outcomes framework (Rubin, 2005). We consider a setup with N subjects and assume an underlying data-generating distribution \mathbb{P}_0 , such that $(\mathbf{X}_i, T_i, Y_i(0), Y_i(1)) \sim_{i.i.d.} \mathbb{P}_0$ for $i = 1, \dots, N$. Here, $(Y_i(0), Y_i(1))$ represents the potential outcomes for subject i . The binary treatment indicator is denoted by $T_i \in \{0, 1\}$, where $T_i = 0$ indicates that subject i received the control, and $T_i = 1$ indicates that subject i received the treatment. The covariates for the i -th subject are represented by a d -dimensional vector $\mathbf{X}_i \in \mathbb{R}^d$. For each subject i , we observe (\mathbf{X}_i, T_i, Y_i) , where $Y_i = T_i \cdot Y_i(1) + (1 - T_i) \cdot Y_i(0)$.

One of the goals in this AD study is to estimate the subgroup average treatment effect (SATE), which can be defined as:

$$\tau(\mathbf{X}_i, \Pi^*) = \sum_{m=1}^{M^*} 1_{(\mathbf{X}_i \in \mathcal{A}_m^*)} \mathbb{E}[Y_i(1) - Y_i(0) | \mathbf{X}_i \in \mathcal{A}_m^*]$$

for subject i . However, directly estimating $\tau(\mathbf{X}_i, \Pi^*)$ is not straightforward because potential outcomes are subject to missingness. To address this, we impose the standard causal identification assumptions:

Assumption H.1 (Consistency). $Y_i = T_i \cdot Y_i(1) + (1 - T_i) \cdot Y_i(0)$.

Assumption H.2 (Unconfoundedness). $(Y_i(0), Y_i(1)) \perp T_i \mid \mathbf{X}_i$.

Under Assumptions H.1 and H.2, the SATE is identifiable in the sense that

$$\tau(\mathbf{X}_i, \Pi^*) = \sum_{m=1}^{M^*} 1_{(\mathbf{X}_i \in \mathcal{A}_m^*)} (\eta_1(\mathbf{X}_i, \mathcal{A}_m^*) - \eta_0(\mathbf{X}_i, \mathcal{A}_m^*)),$$

where $\eta_t(\mathbf{X}_i, \mathcal{A}_m^*) = \mathbb{E}[Y_i | \mathbf{X}_i \in \mathcal{A}_m^*, T_i = t]$ for $t \in \{0, 1\}$.

I Further details on Section 3

I.1 Regression trees and hierarchical partitions

The tree is in one-to-one correspondence with a hierarchy partition (Chatterjee and Goswami, 2021). A hierarchical partition is formed by recursively applying a series of hierarchical splits to the sample space $\mathcal{A} = \prod_{j=1}^d [a_j, b_j]$, where each split involves selecting a coordinate $1 \leq k \leq d$ to be split and then the k -th interval in the product of rectangle \mathcal{A} undergoes this hierarchical split. A hierarchical split of \mathcal{A} produces two sub-rectangles \mathcal{A}_1 and \mathcal{A}_2 where \mathcal{A}_1 takes the form $\mathcal{A}_1 = \prod_{j=1}^{k-1} [a_j, b_j] \times [a_k, l] \times \prod_{j=k+1}^d [a_j, b_j]$ for some $1 \leq k \leq d$ and $a_k \leq l \leq b_k$ and $\mathcal{A}_2 = \mathcal{A} \cap \mathcal{A}_1^c$.

I.2 Intuition on the optimization problem (2)

To provide intuition on the optimization problem (2) and relate it to the tree-based subgroup analysis, we consider a simple case with $M^* = 2$ subgroups induced by a single hierarchical split of the covariate space. In this scenario, the optimization problem (2) simplifies to:

$$\hat{\gamma}_1, \hat{\gamma}_2, \hat{\mathcal{A}}_1, \hat{\mathcal{A}}_2 = \arg \min_{\mathcal{A}_1, \mathcal{A}_2; \gamma_1, \gamma_2 \in \mathbb{R}^{2d+2}} L_n(\gamma_1, \gamma_2, \mathcal{A}_1, \mathcal{A}_2),$$

$$L_n(\gamma_1, \gamma_2, \mathcal{A}_1, \mathcal{A}_2) = \sum_{i=1}^n 1_{(\mathbf{X}_i \in \mathcal{A}_1)} \|Y_i - \gamma_1^T \mathbf{Z}_i\|_2^2 + \sum_{i=1}^n 1_{(\mathbf{X}_i \in \mathcal{A}_2)} \|Y_i - \gamma_2^T \mathbf{Z}_i\|_2^2. \quad (4)$$

where \mathcal{A}_1 and \mathcal{A}_2 are produced by a hierarchical split of the sample covariate space \mathcal{A} . This optimization problem is indeed equivalent to performing a single split in the regression tree with the splitting criteria being the goodness-of-fit measure for the outcome regression model η_t . Thus, solving the optimization problem (2) is equivalent to finding an optimal causal tree that best fits the data and the solution yields a natural estimator of $\tau(\mathbf{X}_i, \Pi^*)$:

$$\hat{\tau}(\mathbf{X}_i, \hat{\Pi}) = \sum_{m=1}^{\hat{M}(\hat{\Pi})} 1_{(\mathbf{X}_i \in \hat{\mathcal{A}}_m)} \cdot (\hat{\mu}_m + \hat{\beta}_m^\top \hat{\mathbf{X}}_m).$$

J A simple example to illustrate how fusion constraint helps the SATE estimation

This localized approach can hamper both subgroup identification and causal effect estimation.

To illustrate this, let us consider a simple example:

$$Y = \sum_{m=1}^M l_m(\boldsymbol{\gamma}_m, \mathbf{Z}_i) \cdot \mathbf{1}_{\mathbf{X} \in \mathcal{A}_m} + \epsilon.$$

where $l_m(\boldsymbol{\gamma}_m, \mathbf{Z}_i) = \mu_m T + \alpha_{1m} X_1 + \alpha_{2m} X_2 + \beta_{1m} T X_1 + \beta_{2m} T X_2$. Under this model, the SATE for \mathcal{A}_m is:

$$\tau(\mathcal{A}_m) = \mu_m + \beta_{1m} \mathbb{E}[X_1 | \mathbf{X} \in \mathcal{A}_m] + \beta_{2m} \mathbb{E}[X_2 | \mathbf{X} \in \mathcal{A}_m].$$

We assume some parameters are homogeneous across different subgroups in this model, while others remain heterogeneous. For example, $\beta_{2,m} = \beta_2$ for all m . In this scenario, the SATE and the relationship between outcomes and covariates can still vary across subgroups. However, relying solely on local data for estimation will lead to less accurate estimation. To see this, we provide further investigations below:

If the estimated subgroups and parameters are $\hat{\mathcal{A}}_m$ and $(\hat{\mu}_m, \hat{\beta}_{1,m}, \hat{\beta}_{2,m})$, the SATE is estimated by:

$$\hat{\tau}(\hat{\mathcal{A}}_m) = \hat{\mu}_m + \hat{\beta}_{1m} \bar{X}_1(\hat{\mathcal{A}}_m) + \hat{\beta}_{2m} \bar{X}_2(\hat{\mathcal{A}}_m),$$

where $\bar{X}_1(\hat{\mathcal{A}}_m)$ and $\bar{X}_2(\hat{\mathcal{A}}_m)$ are the sample means within $\hat{\mathcal{A}}_m$. The local estimation nature of the tree algorithm can impair $\hat{\tau}(\hat{\mathcal{A}}_m)$ in two ways: (1) Estimation within individual leaves may involve limited observations, causing overfitting and inaccurate estimates of parameters such as $\hat{\beta}_{2,m}$. (2) Constructing a decision tree involves a dynamic interplay between tree partitioning and local node estimation. Such an overfitting issue in local node parameter estimation can further reduce subgroup identification accuracy. This claim is validated in our

simulations presented in Section 5.